catalysts

MDPI

Review

Hydrogenation of Carbon Dioxide to Value-Added Chemicals by Heterogeneous Catalysis and Plasma Catalysis

Miao Liu [1], Yanhui Yi [1,2,*], Li Wang [3], Hongchen Guo [1] and Annemie Bogaerts [2]

1 State Key Laboratory of Fine Chemicals, School of Chemical Engineering, Dalian University of Technology, Dalian 116024, China; liumiao_dlut@163.com (M.L.); hongchenguo@163.com (H.G.)
2 Research Group PLASMANT, Department of Chemistry, University of Antwerp, Universiteitsplein 1, BE-2610 Wilrijk-Antwerp, Belgium; annemie.bogaerts@uantwerpen.be
3 College of Environmental Sciences and Engineering, Dalian Maritime University, Dalian 116026, China; liwang@dlmu.edu.cn
* Correspondence: yiyanhui@dlut.edu.cn; Tel.: +86-411-8498-6120

Received: 3 February 2019; Accepted: 8 March 2019; Published: 18 March 2019

Abstract: Due to the increasing emission of carbon dioxide (CO_2), greenhouse effects are becoming more and more severe, causing global climate change. The conversion and utilization of CO_2 is one of the possible solutions to reduce CO_2 concentrations. This can be accomplished, among other methods, by direct hydrogenation of CO_2, producing value-added products. In this review, the progress of mainly the last five years in direct hydrogenation of CO_2 to value-added chemicals (e.g., CO, CH_4, CH_3OH, DME, olefins, and higher hydrocarbons) by heterogeneous catalysis and plasma catalysis is summarized, and research priorities for CO_2 hydrogenation are proposed.

Keywords: carbon dioxide; hydrogenation; heterogeneous catalysis; plasma catalysis; value-added chemicals; methanol synthesis; methanation

1. Introduction

Climate changes are mostly induced by the greenhouse effect, and carbon dioxide (CO_2) accounts for a dominant proportion of this greenhouse effect. Indeed, one can barely ignore the connection between the emission of CO_2 and climate changes [1]. The CO_2 concentration in the atmosphere has actually climbed to 405 ppm in 2017, as shown in Figure 1a. As the global energy consumption is still mainly based on burning coal, oil, and natural gas, and this situation will last until the middle of the century (see Figure 1b), experts predict that the CO_2 concentration in the atmosphere will continue to rise to ~570 ppm by the end of the century if no measures are taken [2]. Hence, it is urgent to control the CO_2 emissions by taking effective measures to capture and utilize CO_2.

In principle, there are three strategies to reduce CO_2 emissions, i.e., reducing the amount of CO_2 produced, storage of CO_2, and utilization of CO_2 [3]. Recently, some comprehensive reviews have discussed the technological state-of-the-art of carbon capture and storage (CCS) [4–6]. Direct air capture technology (DAC) draws people's attention to mitigate climate change by taking advantage of chemical sorbents (e.g., basic solvents, supported amine and ammonium materials, etc.) [4]. In addition, Bui et al. also considered the economic and political obstacles in terms of the large-scale deployment of CCS [6]. Significantly reducing the amount of CO_2 produced is unrealistic in view of the current energy structure dominated by fossil energies, as shown in Figure 1b. CO_2 storage seems to be a potential approach, but there are some challenges, such as efficiency of capture and sequestration of CO_2, cutting down the operation costs for capture and separation of CO_2, and the long-term stability of underground storage [7,8]. Utilization of CO_2 is a promising approach, since CO_2 is a cheap and

attractive carbon source, which can be used to yield a variety of industrial raw materials, which can be further converted into value-added chemicals and fuels. Interestingly, CO_2 can also be used as a desired trigger for stimuli-responsive materials. Darabi et al. summarized the synthesis, self-assembly, and applications of CO_2-responsive polymeric materials [9].

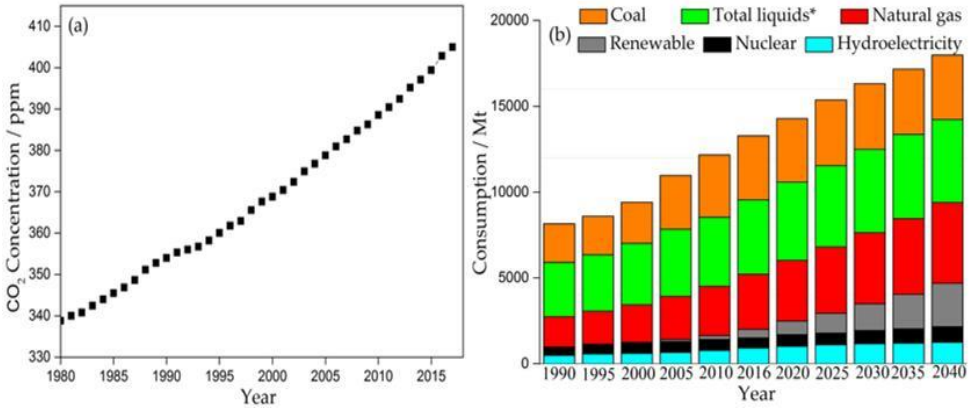

Figure 1. (**a**) Trends in atmospheric CO_2 concentrations (ppm). (**b**) Projected global energy consumption (Mt) from 1990 to 2040. Data from International Energy Agency.

One of the options to convert CO_2, is catalytic hydrogenation, as illustrated in Figure 2. The production of H_2, however, is also a vital problem to realize direct hydrogenation of CO_2 to oxygenates and hydrocarbons. Hydrogen production can be either based on renewable or non-renewable sources, such as electrical, thermal, photonic, and hybrid [10,11]. The main methods of hydrogen production include electrolysis, thermolysis, photo-electrolysis, and hybrid thermochemical cycles [10]. According to some evaluation criteria—such as global warming potential (GWP), social cost of carbon (SCC), acidification potential (AP), energy and exergy efficiencies, and production cost—the hybrid hydrogen production methods seems a promising route. On the other hand, the production cost evaluation shows that coal gasification ($0.92/kg H_2) and fossil fuel reforming ($0.75/kg H_2) are relatively low-cost methods compared to early R&D phase methods (e.g., photo-electrochemical: $10.36/kg H_2 from water dissociation). However, fossil fuel is non-renewable, being a major drawback. Therefore, reducing the cost of hydrogen production is an urgent and challenging issue, since we have to balance both the economy and sustainability.

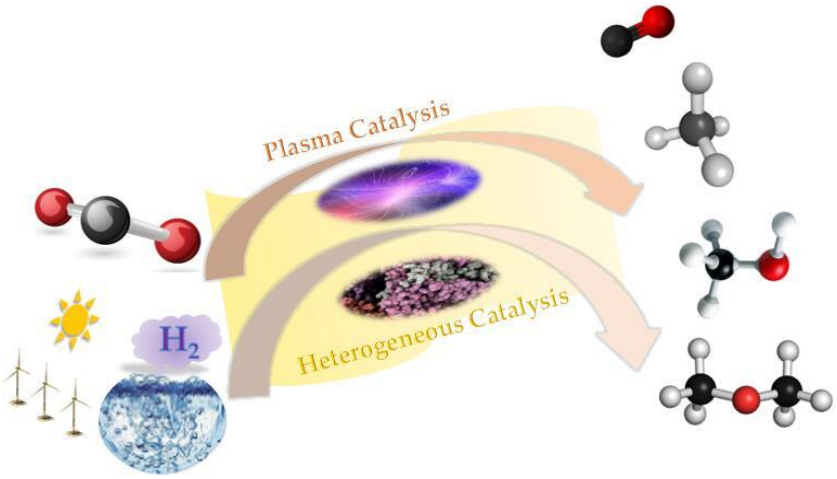

Figure 2. Catalytic hydrogenation of carbon dioxide.

Various methods have been adopted—including photo-catalysis, electro-catalysis, heterogeneous catalysis, and plasma catalysis [12,13]—to realize hydrogenation of CO_2. Dalle et al. systematically

presented the activity of the first-row transition metal complexes (i.e., Sc, Ti, V, Cr, Mn, Fe, Co, Ni, Cu, Zn) in CO_2 reduction by electro-catalysis, photo-catalysis and photoelectron-catalysis [14]. Li et al. discussed the important roles of co-catalysts (e.g., biomimetic, metal-based, metal-free, and multifunctional) in selective photo-catalytic CO_2 reduction [15]. Besides thermochemical approaches, Mota et al. made a detailed retrospective based on electrochemical and photo-chemical approaches for CO_2 hydrogenation to oxygenates and hydrocarbons [16]. In this review, we focus on the latter two methods. Heterogeneous catalysis has been widely studied, while plasma catalysis is still an emerging technology. Some excellent reviews were recently published for heterogeneous catalytic CO_2 hydrogenation [12,17,18]. Jadhav et al. focused on methanol production [17], Porosoff et al. on the synthesis of CO, CH_3OH, and hydrocarbons [18], while Alvarez et al. discussed the greener preparation of formates (formic acid), CH_3OH, and DME [12]. With regard to plasma catalysis for CO_2 hydrogenation, there are only a handful reports (as discussed below). Nevertheless, it exhibits great potential since plasma can operate at ambient temperature and atmospheric pressure.

In this review, we summarize the progress of mainly the last five years in CO_2 hydrogenation to value-added chemicals (e.g., CO, CH_4, CH_3OH, DME, olefins, and higher hydrocarbons) driven by both heterogeneous catalysis and plasma catalysis. The literature bibliography range is shown in Figure 3. Indeed, on the one hand, the insights obtained by heterogeneous catalysis can be useful for the further development of the emerging field of plasma catalysis. On the other hand, we also want to pinpoint the differences between heterogeneous and plasma catalysis, and thus the need for dedicated design of catalytic system tailored to the plasma environment.

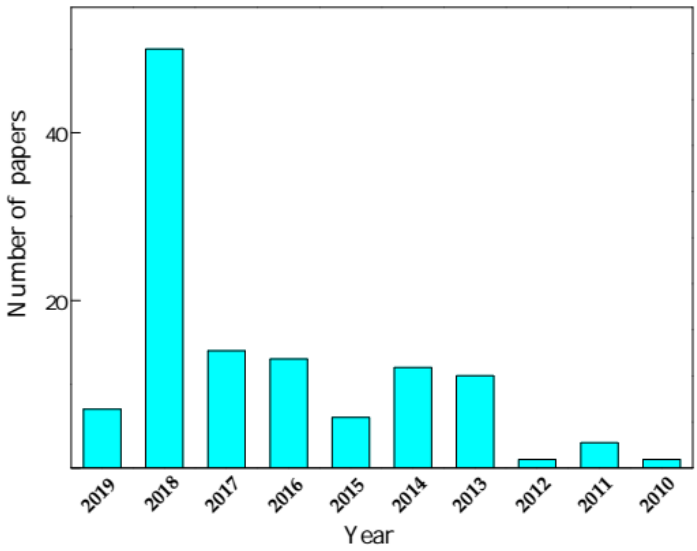

Figure 3. Literature bibliography included in this review.

2. Heterogeneous Catalysis

In heterogeneous catalysis, support materials, active metals, promoters, and the preparation methods of catalysts are major adjustable factors determining the catalytic activity. As far as the support materials are concerned, the catalytic performance is influenced by the metal-support interaction since it usually induces specific physicochemical properties for catalysis, e.g., active cluster, active oxygen vacancy, and acid-based property. Metal oxides and zeolites with special channel structures are usually selected. For the active metal components, research focuses on searching cheap and available metals to replace precious metals or to reduce the amount of precious metals in industrial heterogeneous catalysis. Promoters (structural-type and electron-type) can also significantly influence the catalytic activity by regulating the adsorption and desorption behavior of molecules (reactant, intermediate, and product) on the catalyst surface. Preparation methods usually determine the catalyst morphology including metal dispersion (particle size distribution), specific surface area, and channel structure,

which also influences the catalytic performance [12]. In this section, we summarize recent progress of CO_2 hydrogenation to CO, CH_4, CH_3OH, and some other products in terms of rational design of heterogeneous catalysts.

2.1. CO_2 to CO

CO can be used as feedstock to produce liquid fuels and useful chemicals by Fischer–Tropsch (F–T) synthesis reaction. Therefore, the catalytic hydrogenation of CO_2 to CO via the reverse water–gas shift (RWGS) reaction, reaction (1), is promising to account for the shortage of energy. Accordingly, catalyst design for the RWGS reaction have attracted extensive attention.

$$CO_2 + H_2 \leftrightarrow CO + H_2O, \triangle H_{298K} = 41.2 \text{ kJ mol}^{-1} \quad (1)$$

Generally, noble metal catalysts (e.g., Pt, Ru, and Rh) exhibit effective ability towards H_2 dissociation, and thus precious metals have been investigated extensively for the RWGS reaction. However, these catalysts yield, methane as dominant product, mainly caused by the higher rate of C-H bond formation than CO desorption [19]. To change the product distribution, Bando et al. applied Li-promoted Rh ion-exchanged zeolites for CO_2 hydrogenation, achieving 87% CO selectivity for an atomic ratio of Li/Rh higher than 10/1 [19]. Although the catalytic performance of noble metals can be improved via promoters, the high price and instability of noble metals (aggregation of nano-particles) limit the industrial applicability. In order to properly decrease the operation cost and improve the life cycle of catalysts, non-noble metal carbides have been developed. Porosoff et al. synthesized a molybdenum carbide (Mo_2C) catalyst for the RWGS reaction [20], yielding 8.7% CO_2 conversion and 93.9% CO selectivity (at 573 K reaction temperature). The catalytic performance was much better than those of bimetallic catalysts (e.g., Pt-Co, Pt-Ni, Pd-Co, Pd-Ni) supported on CeO_2 (~5% CO_2 conversion and 83.3% CO selectivity at the same reaction temperature). The catalytic mechanism of Mo_2C in the RWGS reaction was further studied by ambient pressure X-ray photoelectron spectroscopy (AP-XPS) and in situ X-ray absorption near edge spectroscopy (XANES), which demonstrate that Mo_2C not only broke the C=O bond, but also dissociated hydrogen. Hence, Mo_2C has a dual functional and is an ideal catalytic material for the RWGS reaction. Interestingly, the authors also found that by modifying the catalyst with Co, the catalytic activity of the Co-Mo_2C catalyst was further improved (9.5% CO_2 conversion, 99% CO selectivity at 573 K), probably attributed to the existence of the $CoMoC_yO_z$ phase confirmed by X-ray Diffraction (XRD) (see Figure 4).

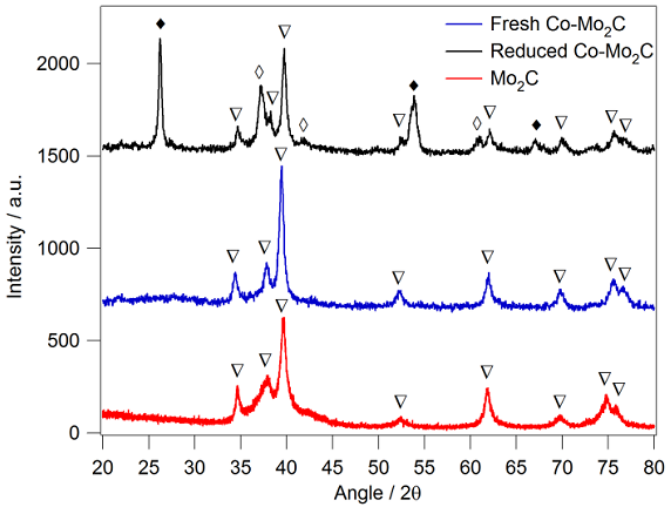

Figure 4. XRD pattern of fresh and reduced Co-Mo_2C with Mo_2C as a reference. The symbols correspond to the following: ▽—β-Mo_2C, ◊—$CoMoC_yO_z$, ♦—MoO_2, reproduced with permission from [20]. Copyright Wiley-VCH, 2014.

The support plays an important role in CO_2 hydrogenation to CO through the RWGS reaction. Kattel et al. prepared Pt, Pt/SiO_2 and Pt/TiO_2 materials as catalysts for the RWGS reaction [21], and showed that Pt nanoparticles alone cannot catalyze the RWGS reaction, while using SiO_2 and TiO_2 as support, the overall CO_2 conversion can be significantly improved, pointing towards a synergy effect between Pt and the oxide support. To reveal the synergy effect, they combined density functional theory (DFT), kinetic Monte Carlo (KMC) simulations and other experimental measurements. They found that the hydrogenation of CO_2 to CO is promoted once CO_2 is stabilized by the Pt-oxide interface. In the case of Pt nanoparticles (NP) alone, the conversion was close to 0, since the ability of Pt NP in binding CO_2 is weak. When SiO_2 and defected TiO_2 with oxygen vacancies served as supports, however, the CO_2 conversion was enhanced (to 3.35% and 4.51%, respectively) on the Pt-oxide interface. The synergy effect between Pt and oxide supports in activating and hydrogenating CO_2 is shown in Figure 5, and possible reaction pathway [21] for the RWGS reaction is illustrated in Scheme 1.

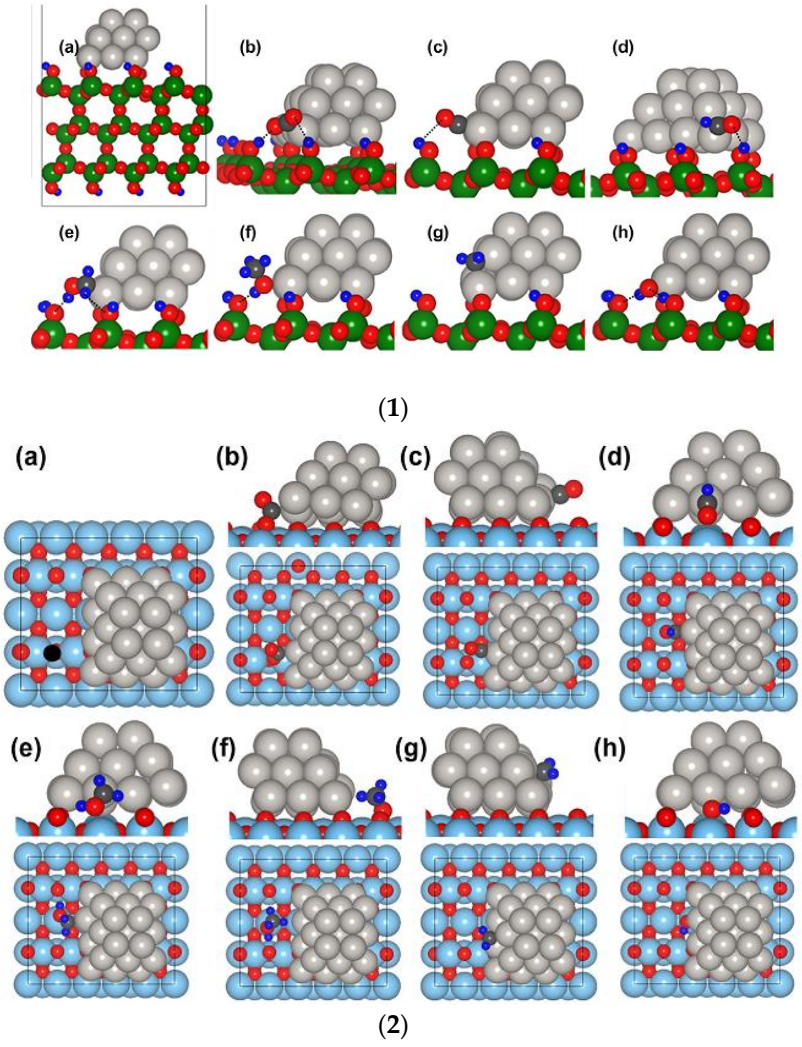

Figure 5. DFT optimized geometries. (**1**) (**a**) Pt_{25}/hydroxylated SiO_2 (111), and (**b**) $*CO_2$ species, (**c**) *CO species, (**d**) *HCO species, (**e**) $*H_2COH$ species, (**f**) $*CH_3OH$ species, (**g**) $*CH_2$ species, and (**h**) *OH species adsorbed on Pt/SiO_2 (111). The dashed lines show hydrogen bonds. (**2**) (**a**) Pt_{25}/TiO_2 (110) with oxygen vacancy, and side (**top**) and top (**bottom**) views of (**b**) $*CO_2$ species, (**c**) *CO species, (**d**) *HCO species, (**e**) $*H_2COH$ species, (**f**) $*CH_3OH$ species, (**g**) $*CH_2$ species, and (**h**) *OH species adsorbed on Pt/TiO_2 (110). The black circle in (a) depicts the position of oxygen vacancy on TiO_2 (110). Note: Si: green, Ti: light blue, Pt: light gray, C: dark gray, O: red, and H: blue, reprinted with permission from [21]. Copyright Elsevier, 2016.

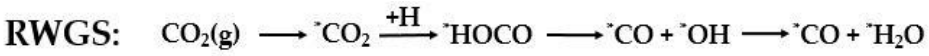

Scheme 1. Reaction pathways for the RWGS reaction, where '*X' represents species X adsorbed on a surface site, reproduced with permission from [21]. Copyright Elsevier, 2016.

Yan et al. investigated the effect of the Ru-Al_2O_3 interfaces on the catalytic activity of the RWGS reaction, and proposed Ru_{35}/Al_2O_3 and Ru_9/Al_2O_3 catalyst models to explain the experimental observations [22]. The product selectivity switched between CH_4 and CO over the Ru/Al_2O_3 catalyst, i.e., monolayer Ru sites favored the production of CO, while Ru nano-clusters preferred the production of CH_4, during CO_2 reduction reaction. Confirmed by kinetic analysis, characterization of the surface structures and real-time monitoring of the active intermediate species, the product selectivity of CH_4 and CO was regulated by the Ru sites and Ru-Al_2O_3 interfacial sites. Furthermore, based on the combination of theoretical calculations and isotope-exchange experimental results, the authors found that the O* species derived from the dissociative adsorption of CO_2 at interfacial Ru sites easily bridge with the Al sites from the γ-Al_2O_3 support, and new Ru-O-Al bonds are formed via the oxygen-exchange process. The interfacial O species existing in Ru-O-Al bonds was responsible for the CO_2 activation via oxygen-exchange with the O atoms of CO_2. Therefore, this experimental work is a good inspiration to further explore the influence of metal-support interfaces for the effective activation of CO_2.

Besides the widely used impregnation method, Yan et al. also reported a doping-segregation method for the preparation of Rh-doped $SrTiO_3$ [23]. Precursors with a molar ratio of Sr:Ti:Rh = 1.10:0.98:0.02. First, TiO_2 was suspended in deionized water, and then $Sr(OH)_2{\cdot}8H_2O$ and $Rh(NO_3)_3$ were introduced. Subsequently, the sample was poured in a stain steel acid digestion vessel, which was kept at 473 K for 24–48 h. Finally, the reaction product was dried at 343 K overnight after it was centrifuged, and washed via deionized water. As confirmed by in situ X-Ray-Diffraction (XRD) and X-ray Absorption Fine Structure (XAFS) measurements, the Rh-doped $SrTiO_3$ catalysts produce sub-nanometer Rh clusters, which are highly active for the conversion of CO_2 compared to the supported $Rh/SrTiO_3$ prepared by wetness impregnation. The better catalytic performance (7.9% CO_2 conversion and 95% CO selectivity at 573 K) could be ascribed to the cooperative effect between sub-nanometer Rh clusters and the reconstructed $SrTiO_3$ which is active for dissociation of H_2 and is favorable for adsorption/activation of CO_2. Therefore, the novel approach, doping-segregation method, maybe a novel strategy to tune the size of active metals and the physicochemical properties of supports for rational design of catalysts for the RWGS reaction.

Dai et al. studied CeO_2 catalysts which were prepared by the hard-template method (Ce-HT), the typical complex method (Ce-CA), and the typical precipitation method (Ce-PC) for the RWGS reaction [24]. The experimental results show that catalysts prepared by Ce-CA, Ce-HT, and Ce-PC methods exhibit a 100% CO selectivity and the CO_2 conversions were 9.3, 15.9, and 12.7% respectively at 853 K. Obviously, the hard-template (Ce-HT) method is beneficial for the RWGS reaction in view of the catalytic performance. The Ce-HT method comprises the following steps: (1) $Ce(NO_3)_3{\cdot}6H_2O$ was dissolved in ethanol, and KIT-6 mesoporous silica was added; (2) The mixture was stirred until a dry power was obtained; (3) The powder was calcined; (4) The obtained samples were treated with NaOH to remove the template. To reveal the relationship between the preparation method and the catalytic activity, the authors carried out XRD, Transmission Electron Microscopy (TEM) and Brunauer–Emmett–Teller (BET) characterization, and the characterization results show that CeO_2 catalysts which were prepared by the Ce-HT method have a porous structure and a high specific surface area, while CeO_2 catalysts prepared by the other methods (Ce-CA, Ce-PC) have an agglomerated structure (Ce-CA) and overlapped bulk structure (Ce-PC) with low porosity. Moreover, in the CeO_2 catalysts, oxygen vacancies as active sites were formed by H_2 reduction at 673 K, which were confirmed by in situ X-ray photoelectron spectroscopy (XPS) and H_2-temperature-programmed reduction (H_2-TPR). Therefore, the improvement of the catalytic activity for the RWGS reaction can be ascribed to the change of catalyst structure and oxygen vacancies.

Except for the above monometallic catalysts, some bimetallic catalysts—i.e., Pt-Co, Fe-Mo and Ni-Mo [25–27]—were also prepared and tested in the RWGS reaction. In general, the preparation method of bimetallic catalysts generally can be divided into two categories: (1) the bi-metal was first prepared and then supported on the carrier [25]; (2) the bi-metal as formed in the preparation progress [26,27]. Compared with pure Co catalyst, Pt-Co catalyst showed a better catalytic activity (mainly CO, close to 100%) for the RWGS reaction. Ambient pressure X-ray photoelectron spectroscopy (AP-XPS) and environmental transmission electron microscopy (ETEM) showed that Pt migrates on the catalyst surface, and Pt aids the reduction of Co to its metallic state under appropriate reaction conditions confirmed by near edge X-ray absorption fine structure (NEXAFS) spectroscopy [25]. Abolfazl et al. investigated Mo/Al_2O_3 and $Ni–Mo/Al_2O_3$ catalysts prepared by the impregnation method used for the RWGS reaction. The experimental results showed that $Ni–Mo/Al_2O_3$ catalyst is a promising catalyst (35% CO_2 conversion, i.e., close to the 38% equilibrium conversion) compared with Mo/Al_2O_3 catalyst (15% CO_2 conversion). As demonstrated by XPS, the electronic effect, which transfers electrons from Ni to Mo and leads to an electron-deficient state of the Ni species, is beneficial for CO_2 adsorption, and thus improves the CO_2 conversion. Furthermore, the XRD and H_2-TPR profiles indicated that the Ni–O–Mo structure crystallizes into the $NiMoO_4$ phase which can improves the adsorption and dissociation of H_2 on the $Ni-Mo/Al_2O_3$ catalyst [27]. Similarly, they also found that $Fe-Mo/Al_2O_3$ catalyst synthesized by the impregnation method is an efficient catalyst with high CO yield, almost no by-products and relatively stable (60 h) for the RWGS reaction. The enhancement of the catalytic activity may be attributed to better Fe dispersion with the addition of Mo and smaller particle size of active Fe species, which was confirmed by the BET method and scanning electron microscopy (SEM) [26].

Overall, to some extent, the reaction activity and stability of bimetallic catalysts for the direct hydrogenation of CO_2 to CO are excellent compared to mono-metallic catalysts. The reduction of the active metal, the formation of alloy metal, the dispersion and particle size of the catalyst are possible factors for the improvement of the catalytic performance in the RWGS reaction. Details of the conversion and product selectivity, along with the reaction conditions of several representative RWGS catalytic systems, are compared in Table 1. Obviously, precious metal catalysts (e.g., Pt, Rh, Ni) are still advantageous for the formation of CO compared to non-noble metal catalysts (e.g., Fe, Co, Mo), and upon increasing the gas hourly space velocity (GHSV), the selectivity of CO slightly decreases to some extent.

Table 1. Catalytic performance of several catalytic systems for CO_2 hydrogenation into CO, in terms of CO_2 conversion and CO selectivity, along with the reaction conditions

Catalyst	H_2:CO_2	GHSV	Temperature (°C)	Pressure (MPa)	CO_2 Conversion (%)	CO Selectivity (%)
Mo_2C [20]	3	36,000 [a]	300	0.1	8.7	93.9
Co-Mo_2C [20]	3	36,000 [a]	300	0.1	9.5	~99.0
Pt-TiO_2 [21]	1	119.7 [b]	300	0.1	4.5	99.1
Pt-SiO_2 [21]	1	24.7 [b]	300	0.1	3.3	100
Rh-$SrTiO_3$ [23]	1	12,000 [a]	300	N/A	7.9	95.4
Co-MCF-17 [25]	3	60,000 [b]	200-300	0.5	~5.0	~90.0
Pt-Co-MCF-17 [25]	3	60,000 [b]	200-300	0.5	~5.0	~99.0
Fe-Mo-Al_2O_3 [26]	1	30,000 [a]	600	1	~45.0	~100.0
Mo-Al_2O_3 [27]	1	30,000 [a]	600	0.1	16	N/A
Ni-Mo-Al_2O_3 [27]	1	30,000 [a]	600	0.1	34	N/A
La-Fe-Ni [28]	2	24,000 [a]	350	N/A	16.3	96.6

[a] mL g_{cat}^{-1} h^{-1}; [b] h^{-1}; N/A: not available.

2.2. CO_2 to CH_4

Methane, a high value carbon source, is used to produce syngas via steam reforming, and subsequently the syngas is usually converted into chemicals and/or fuels through F–T synthesis.

The direct hydrogenation of CO_2 to CH_4 (also called CO_2 methanation), reaction (2), is a feasible approach, if the production technology of H_2 becomes widespread and at low-cost.

$$CO_2 + 4H_2 \leftrightarrow CH_4 + 2H_2O, \triangle H_{298K} = -252.9 \text{ kJ mol}^{-1} \quad (2)$$

Ni-based [29], Co-based [30], and Ru-based [31] catalysts have been used in CO_2 methanation, and Ni-based catalysts are considered to be the most effective and the lowest cost alternative. However, coke formation is a serious problem for Ni-based catalytic systems [2]. Therefore, researchers are trying to seek appropriate promoters to improve the activity and stability of Ni-based catalytic systems for CO_2 methanation. Yuan et al. investigated the effect of Re on the catalytic activity of Ni-based catalysts in CO_2 methanation [32]. Based on DFT calculations, they found that, attributed to the strong affinity of Re to O (see Figure 6), the presence of Re markedly lowered the energy barrier of C-O bond cleavage, which benefits the activation of CO_2. Moreover, CH_4 selectivity can be enhanced owe to the presence of Re, which was confirmed by analysis of surface coverage of the adsorbed species on Ni (111) and Re@Ni (111). In addition, micro-kinetic analysis showed that, in addition to CO* and H*, a suitable amount of O_{ad} atoms were present on Re@Ni (111), and thus a possible reaction network of CO_2 methanation was proposed as shown in Scheme 2, in which a red line represents the preferable steps in each pathway.

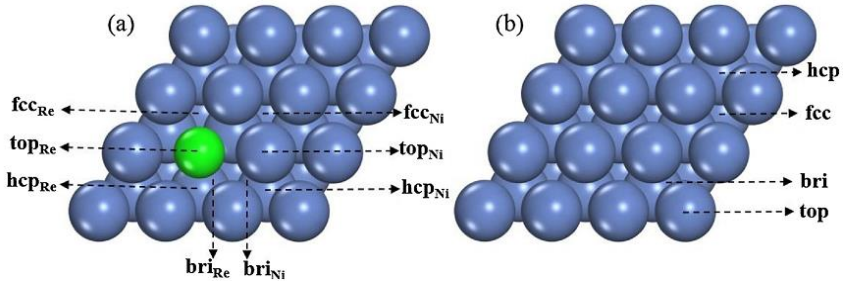

Figure 6. Adsorption sites existed in the (**a**) Re@Ni(111) and (**b**) Ni(111) surface. Ni: blue, Re: green, reprinted with permission from [32]. Copyright Elsevier, 2018.

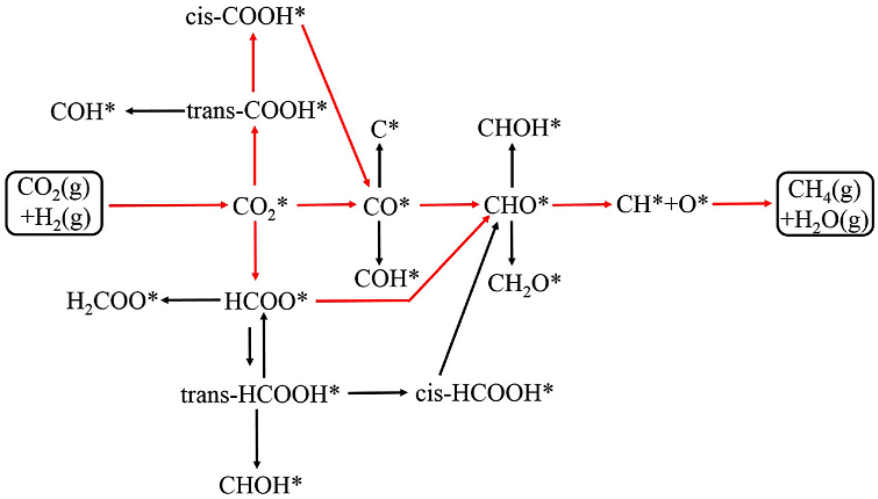

Scheme 2. Reaction network for CO_2 methanation. The preferable steps in each pathway are marked with a red line, reproduced with permission from [32]. Copyright Elsevier, 2018.

Besides Re, La is also an excellent promoter of Ni-based catalysts for CO_2 methanation. Quindimil et al. [29] applied Ni-La_2O_3/Na-BETA catalysts for CO_2 methanation. They found that the presence of La_2O_3 created more CO_2 adsorption sites and more hydrogenation sites, mainly attributed to the improved surface basicity and Ni dispersion by the co-catalyst effect of La. Under the optimized

reaction conditions, 65% CO_2 conversion and nearly 100% CH_4 selectivity were achieved over a Ni-10%La_2O_3/Na-BETA catalyst with a good stability for more than 24 h at 593 K.

CeO_2, TiO_2, and SiO_2 have been used as the supports of methanation catalysts [33]. Reactions over Ni/CeO_2 catalyst performed full selectivity to CH_4 with higher TOF (up to forty-fold) compared to TiO_2 and SiO_2 supported Ni nanoparticles, and in CO_2 methanation, the catalytic stability of Ni/CeO_2 catalyst lasted for 50 h at 523 K. HRTEM analysis indicated that different supports induced distinctive crystal structure. Ni/CeO_2 catalyst presented hexagonal Ni nanocrystallites, while TiO_2 and SiO_2 favored the formation of pseudo-spherical Ni nanoparticles. Demonstrated by TPR, XPS, and UV Raman analysis, characterization results revealed partial reduction of the CeO_2 surface, and the partial reduction of the CeO_2 surface contributed to the generation of oxygen vacancies, which is beneficial for the formation of a strong metal-support interaction (SMSI) between Ni and CeO_2, while no SMSI was observed over Ni/SiO_2 and Ni-TiO_2 catalyst. Furthermore, pulse reaction by temporal analysis products (TAP) demonstrated the capacity of CO_2 adsorption following the order: Ni/SiO_2 < Ni/TiO_2 < Ni/CeO_2. Therefore, metal particle morphology and surface oxygen vacancies were used to anchor/stabilize Ni nanoparticles, and SMSI of Ni/CeO_2 catalyst contributed to the remarkable catalytic activity for CO_2 methanation.

Lin et al. investigated the influence of TiO_2 phase structure on the degree of dispersion of Ru nanoparticles [31]. Experiments showed that Ru/r-TiO_2 (rutile-type TiO_2) catalysts have a fast rate of CO_2 conversion, more than twice as fast as Ru/a-TiO_2 (anatase-type TiO_2) for CO_2 methanation. Meanwhile, compared to Ru/a-TiO_2 catalysts, Ru/r-TiO_2 catalysts exhibited a much higher thermal stability. High-angle annular dark-field scanning transmission electron microscopy (HAADF-STEM) images showed that r-TiO_2 supported Ru nanoparticles displayed a narrower particle size distribution (1.1 ± 0.2 nm) compared with a-TiO_2 supported Ru nanoparticles (4.0 ± 2.4 nm). As confirmed by XRD measurements and H_2-TPR experiments, a strong interaction existed in RuO_2 and r-TiO_2 contributed to the formation of the Ru–O–Ti bond. Experimental tests, revealed that the strong interaction between RuO_2 and r-TiO_2, not only promotes the highly dispersion of Ru nanoparticles, but also prevents nanoparticles' aggregation, which is responsible for the enhancement of the catalytic activity and thermal stability.

Furthermore, the influence of Al_2O_3, ZrO_2, SiO_2, KIT-6, and GO supports on Ni-based catalysts [30,34,35] has also been reported recently (Table 2). The specific area of support, the metal-support interaction and particle size of active sites are still mainly adjustable factors. Interestingly, Ni-SiO_2/GO-Ni-foam catalyst which was synthesized via intercalation of graphene oxide (GO) exhibited excellent activity compared with Ni-SiO_2/Ni-foam catalyst (see Figure 7) at 743 K for CO_2 methanation. Furthermore, the formation of nickel silicates on GO is responsible for the uniform dispersion of Ni active sites, which is favorable for inhibition of catalyst sintering.

Table 2. Catalytic performance of several catalysts for CO_2 methanation, in terms of CO_2 conversion and CH_4 selectivity, along with the reaction conditions

Catalyst	H_2:CO_2	GHSV	Temperature (°C)	CO_2 Conversion (%)	CH_4 Selectivity (%)
Ni-La/Na-BETA [29]	4	10,000 [b]	350	65	100
Co/meso-SiO_2 [30]	4.6	60,000 [a]	280	40	94.1
Co/KIT-6 [30]	4.6	22,000 [a]	280	48.9	100
Ru/BF_4/SiO_2 [30]	4	2400 [b]	250	70.5	N/A
Re-Ni(111) [32]	4	N/A	250	N/A	100
Ni/Al_2O_3-ZrO_2 [34]	4	40,000 [a]	400	~70.0	N/A
Ni-SiO_2/GO [35]	4	500 [b]	470	54.3	88
Ni-ZrO_2 [36]	4	75 [a]	350	~40.0	~95.0
Ni-Ce/USY [37]	4	N/A	350	65	95
Co/KIT-6 [38]	4	60,000 [a]	340	40	86.7
Co/SiO_2 [39]	4	60,000 [a]	360	44.3	86.5
Ni-Nb_2O_5 [40]	4	750 [b]	325	81	~99.0

[a] mL g_{cat}^{-1} h^{-1}; [b] h^{-1}; N/A: not available; pressure: 0.1 MPa.

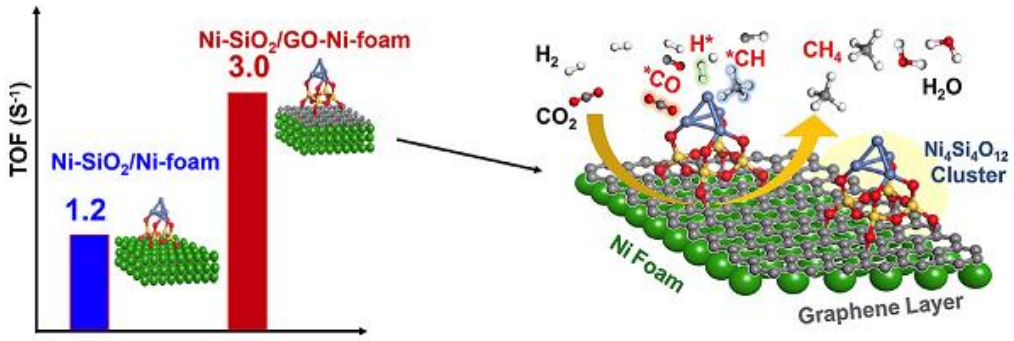

Figure 7. TOF of Ni-SiO_2/Ni-foam and Ni-SiO_2/GO-Ni-foam catalysts for CO_2 methanation, reprinted with permission from [35]. Copyright Elsevier, 2019.

Besides the traditional methods (co-impregnation method and deposition–precipitation method), some novel preparing methods, such as the sequential impregnation and a change of the preparation progress (e.g., the metal incorporation order, the reduction temperature, and the selection of different types of precursors), have been recently reported for preparing methanation catalysts.

Romero-Sáez et al. synthesized Ni-ZrO_2 catalysts supported on CNTs via the sequential and co-impregnation methods for CO_2 methanation [36]. The catalyst prepared by co-impregnation was apparently less active and selective to CH_4, compared with the catalyst synthesized by the sequential impregnation method. The preparation approach of the sequential impregnation method is as follows: (1) the appropriate amount of $ZrO(NO_3)_2$ xH_2O was dissolved in acetone; (2) the CNTs were added to the solution; (3) removal of the solvent, drying and heat treatment at 623 K; (4) in a rotatory evaporator, the same procedure for $Ni(NO_3)_2$ impregnation, followed drying and heat treatment was applied. As characterized by TEM analysis, NiO nanoparticles surrounded by ZrO_2 in core–shell structures were formed via co-impregnation method.The existence of core–shell structure reduced reactant access to Ni and Ni–ZrO_2 interface. However, when the catalyst was prepared via a sequential impregnation method, NiO nanoparticles were available and deposited either on the surface or next to the ZrO_2 nanoparticles, which improved the extent of the Ni–ZrO_2 interface. The ratio of Ni–O–Zr exposed species thus increases in the sequential impregnation method, and the interaction between H atoms (produced upon H_2 dissociation on the Ni surface) and the CO_2 molecule (activated by ZrO_2), can also be enhanced. The schematic representation is shown in Figure 8.

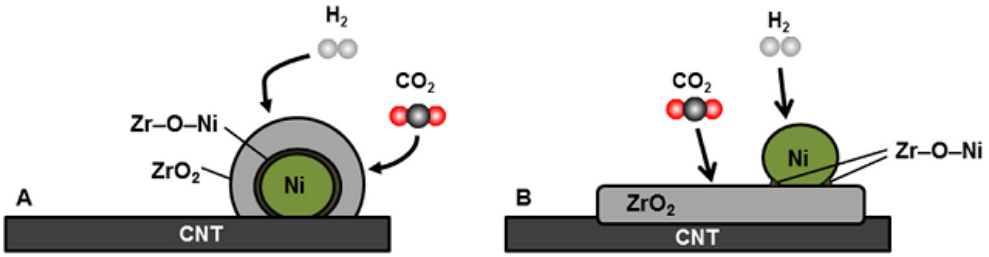

Figure 8. Schematic representation of the disposition of NiO, ZrO_2 and interface Ni-O-Zr at the surface of CNTs for (**A**) Ni-Zr-CNT-COI catalytic system, and (**B**) Ni-Zr-CNT-SEQ catalytic system, reproduced with permission from [36]. Copyright Elsevier, 2018.

Interestingly, Bacariza et al. investigated the influence of the metal incorporation order in the preparation of Ni-Ce/Y(USY) zeolite catalysts [37]. In their experiments, three ways were used for the preparation of catalysts: Ni before Ce (Ce/Ni), Ce before Ni (Ni/Ce), and co-impregnation (Ni-Ce). Experimental tests showed that the catalytic activity follows the order: Ce/Ni ≈ Ni/Ce < Ni-Ce. TEM and H-TPR characterizations demonstrated that the Ni^0 average size decreases to approximately 2.5 nm, and in terms of Ni/Ce or Ni-Ce catalysts, stronger interactions between Ni and Ce species are established. However, the CO_2 adsorption capacity is smaller for Ni/Ce catalyst. In contrast, even

though larger Ni^0 particles (13.3 nm) are formed for Ce/Ni catalyst, CO_2 adsorption capacity can be enhanced. Finally, Ce-Ni was found as the best preparation method for CO_2 methanation using Ni-based catalysts supported on CeO_2.

In addition, it has been reported that the reduction temperature and a variety of different precursors (e.g., nitrate, chlorate, and oxalate) affect the number of active centers for CO_2 methanation [30,38]. As discussed above, the preparation methods showed beneficial influences on the catalytic performance, suggesting that reasonable adjustment of the preparation process is a strategy to optimize the experiments for the conversion of CO_2 to CH_4. Details of CO_2 conversion and product selectivity, along with the reaction conditions of several representative catalytic systems, are compared in Table 2. From Table 2, we can see that Ni-based catalysts are the main catalytic systems for the conversion of CO_2 to CH_4. Furthermore, the optimal temperature for CH_4 production is 300–400 °C.

2.3. CO_2 to CH_3OH

Methanol is not only an important industrial raw material, but also a stable hydrogen storage compound, which is convenient for transport and reserve. Recently, the concept of "methanol economy" advocated by the Nobel Laureate George Olah revealed the importance of methanol in energy structure [41]. Hence, a large amount of heterogeneous catalysts for the direct hydrogenation of CO_2 to CH_3OH, reaction (3), have emerged in recent years. Herein, we summarize some catalytic systems for the direct hydrogenation of CO_2 to CH_3OH (see Figure 9).

$$CO_2 + 3H_2 \leftrightarrow CH_3OH + H_2O, \triangle H_{298K} = -49.5 \text{ kJ mol}^{-1} \quad (3)$$

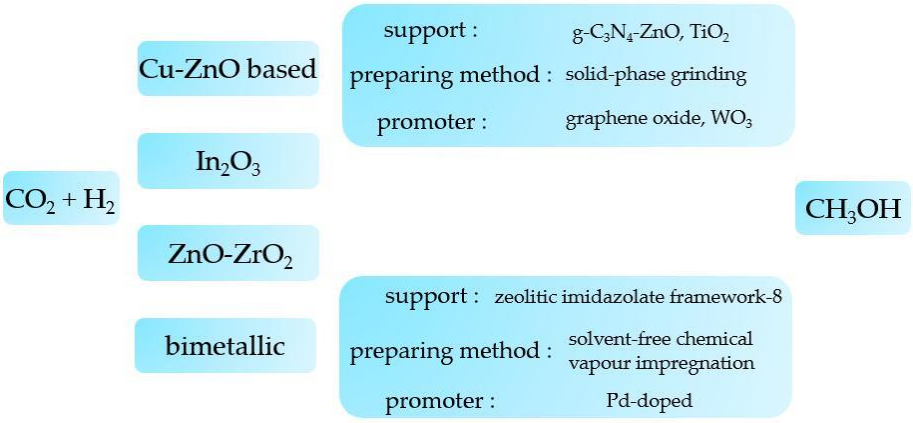

Figure 9. Catalytic system for the direct hydrogenation of CO_2 to CH_3OH in this review.

Cu-ZnO-based catalysts, developed by ICI (Imperial Chemical Industries) in the 1960s, are still widely used in CH_3OH synthesis from syngas (CO and H_2), and Cu^0 is considered to be the active site. Li et al. reported the synthesis of Cu/ZnO catalysts using a unique method, i.e., facile solid-phase grinding, using mixture of oxalic acid, copper nitrate, and zinc nitrate as raw materials [42]. Appropriate amount of these compounds were physically mixed, and then manually ground for 0.5 h. Subsequently, at 393 K, the obtained precursor was dried for 12 h, and at 623 K, calcined for 3 h in N_2 flow, followed by passivation in 1% O_2/N_2 flow for 5 h. In contrast, by the following steps: (1) at 623 K, calcining the dried precursor at for 3 h in air; (2) at 503 K, reducing the oxide for 10 h in 5% H_2/N_2 flow; and (3) at room temperature, passivating the catalyst in 1% O_2/N_2 flow for 5 h, the catalyst can be obtained via H_2 reduction. As demonstrated by XRD, H_2-TPR and thermal-gravity-differential thermal analysis (TG-DTA), in the facile solid-phase grinding process, the decomposition of oxalate complexes and the reduction of CuO took place simultaneously when the samples were calcined in N_2, which prevented the growth of active Cu^0 species and the aggregation of catalyst particles. In contrast, in the

conventional H_2 reduction process, the growth of active species or the aggregation of catalyst particles were inevitable. Notably, Cu/ZnO catalysts prepared by a facile solid-phase grinding method achieved 29.2% CO_2 conversion (at 523 K and 3 MPa), which is even higher than the thermodynamic equilibrium conversion. Indeed, the equilibrium conversion of CO_2 at 473 K and 3 MPa is 25.78% according to the Benedict–Webb–Rubin equation [43], and it is even lower at 523 K, since CO_2 hydrogenation to CH_3OH is an exothermic reaction. Generally, tandem reaction can break the limit of thermodynamic on reaction result. Inspiring from which, the above unusual experimental results (higher than thermal equilibrium value) could be most likely achieved through tandem reactions, in which every stepwise reaction was accelerated by different metal sites. Therefore, the simple and solvent-free method based on solid-phase grinding, opened a new approach to synthesize bimetallic or multimetallic catalysts without further reduction.

To improve the catalytic activity of $Cu/ZnO/Al_2O_3$ catalysts, ZnO was replaced by g-C_3N_4-ZnO hybrid material, as reported by Deng et al. [44]. The experimental results showed that, at 12 bar and 523 K, the methanol space time yield (STY) reached 5.73 mmol h^{-1} $g_{Cu}{}^{-1}$ for Cu- g-C_3N_4-ZnO/Al_2O_3, which is superior to the methanol yield (5.45 mmol h^{-1} $g_{Cu}{}^{-1}$) of industrial catalyst (Cu-ZnO-Al_2O_3) under the same reaction pressure. As confirmed by time-resolved photoluminescence (TRPL) and electronic spin resonance (ESR), the electron-richness of ZnO was enhanced via the formation of type-II hetero-junction between g-C_3N_4 and ZnO. In addition, in the TPR curve, enhanced SMSI was observed, and the SMSI between electron-rich ZnO and Cu could boost the catalytic performance in CH_3OH production. The study provided a viable and economic method to modify traditional catalysts for improving CH_3OH production.

For CuO-ZnO-ZrO_2 catalysts, doping graphene oxide (GO) is a good strategy for improving the activity of CO_2 to CH_3OH [45]. The highest methanol selectivity reached up to 75.88% (473 K, 20 bar) at 1 wt % GO content, while under the same conditions, the methanol selectivity was found to be 68% over the GO-free catalyst. Furthermore, CuO-ZnO-ZrO_2-GO catalyst exhibited an almost constant space-time yield (STY) of methanol after 96 h time-on stream experiment. As demonstrated by H_2-TPD and CO_2-TPD, the CO_2 and H_2 adsorption capacity is enhanced over the CuO-ZnO-ZrO_2-GO catalysts. Additionally, to explain the improvement of catalytic activity, the authors proposed that GO nano-sheet can serve as a bridge between mixed metal oxides, which strengthens a hydrogen spillover (see Figure 10). That is, H species migrating from the copper surface to the carbon species are adsorbed on the isolated metal oxide particles.

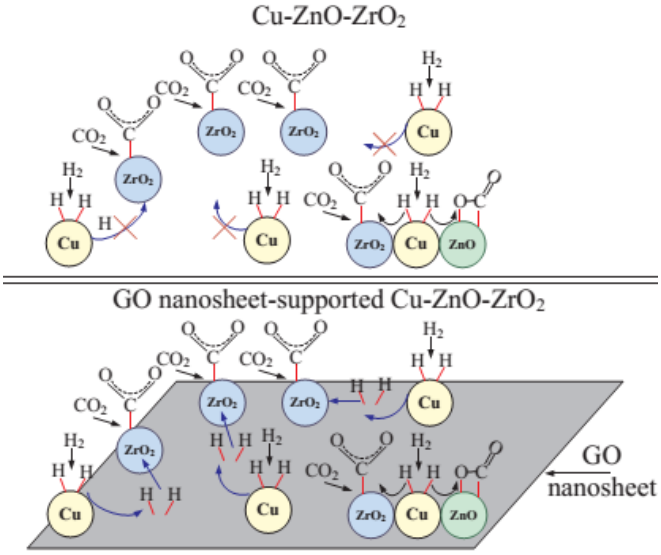

Figure 10. Graphene oxide (GO) nanosheet as a bridge promoting hydrogen spillover from the surface of copper to the surface of other metal oxides, reproduced with permission from [45]. Copyright Elsevier, 2018.

It is also reported that modification by small amounts (2 and 5 at %) of WO_3 can improve the CO_2 conversion and CH_3OH selectivity of the CuO-ZnO-ZrO_2 catalyst [46]. The optimal catalytic performance can be attributed to the specific surface area of metallic Cu, basic sites, and the reducibility of catalysts. However, if we want to effectively tune the catalytic reaction, a better understanding of the reaction mechanisms is essential. Up to now, the possible reaction pathways for the hydrogenation of CO_2 to methanol over Cu-ZnO-based catalysts are shown in Scheme 3.

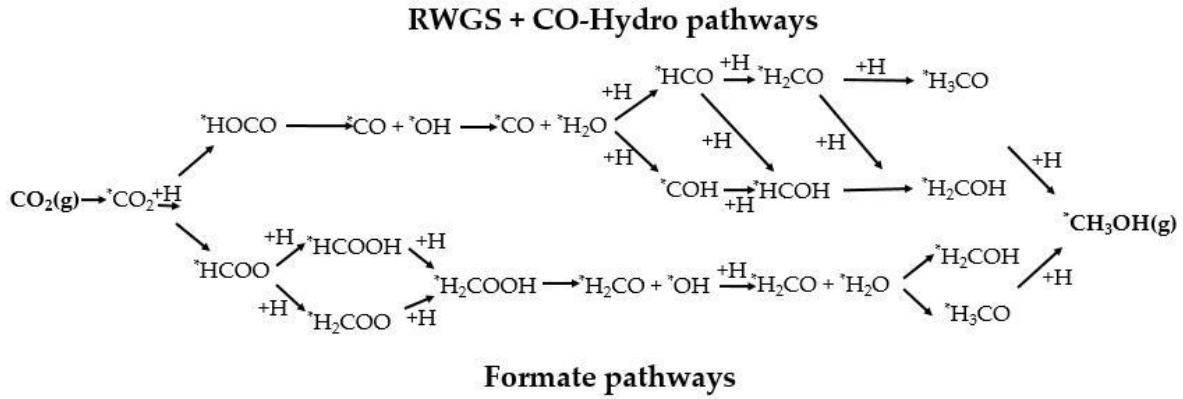

Scheme 3. Possible reaction pathways for CO_2 hydrogenation to methanol, where '*X' represents species X adsorbed on a surface site, reprinted with permission from [21]. Copyright Elsevier, 2016.

Besides Cu-based catalysts, In_2O_3 catalyst with surface oxygen vacancies has attracted more and more attention from researchers. Using density functional theory (DFT) calculations, Ye et al. investigated a In_2O_3 catalyst for the hydrogenation of CO_2 to CH_3OH [47]. On a perfect In_2O_3 (110) surface, six possible surface oxygen vacancies (O_{v1} toO_{v6}) were investigated (see Figure 11a), and the D4 surface with the O_{v4} defective site was found to be most beneficial for CO_2 activation and further hydrogenation. Potential energy profiles of CO_2 hydrogenation and protonation on the D4 defective In_2O_3 (110) surfaces are shown in Figure 11b. In addition, the simulation results showed that the formation of CH_3OH replenishes the oxygen vacancy sites, while H_2 contributes to generate the vacancies, and this cycle between perfect and defective states of the surface is responsible for the formation of CH_3OH from CO_2 hydrogenation. To demonstrate this hypothesis, In_2O_3 catalyst was used for the hydrogenation of CO_2 to CH_3OH in practice, which showed the superior catalytic activity (7.1% CO_2 conversion, 39.7% CH_3OH selectivity at 603 K). This experimental result is better than for many other reported catalytic systems, which generally show low selectivity of CH_3OH at 603 K. Confirmed by thermo-gravimetric analysis (TGA), XRD, and HR-TEM, the authors found that In_2O_3 catalyst had satisfactory thermal and structural stability for CO_2 conversion to CH_3OH below 773 K [48]. Furthermore, to reveal the effect of oxygen vacancies, Martin et al. synthesized bulk In_2O_3 catalyst, and at a wide range of reaction conditions, the CH_3OH selectivity could be tuned up to 100%. XRD, H_2-TPR, CO_2-TPD, XPS, operando diffuse reflectance infrared Fourier transform spectroscopy (DRIFTS), and electron paramagnetic resonance (EPR) characterization confirmed that oxygen vacancies on the In_2O_3 catalyst are active sites for the reduction of CO_2. Additionally, to further improve the stability of In_2O_3 catalyst for the production of CH_3OH, the authors investigated a variety of supports (i.e., ZrO_2, TiO_2, ZnO_2, SiO_2, Al_2O_3, C, SnO_2, MgO). ZrO_2 showed the best catalytic performance since it prevented the sintering of the In_2O_3 phase, which was demonstrated by the enduring stability of In_2O_3/ZrO_2 catalyst over 1000 h [49]. Overall, In_2O_3 is a potential catalyst for CO_2 hydrogenation to CH_3OH with high selectivity.

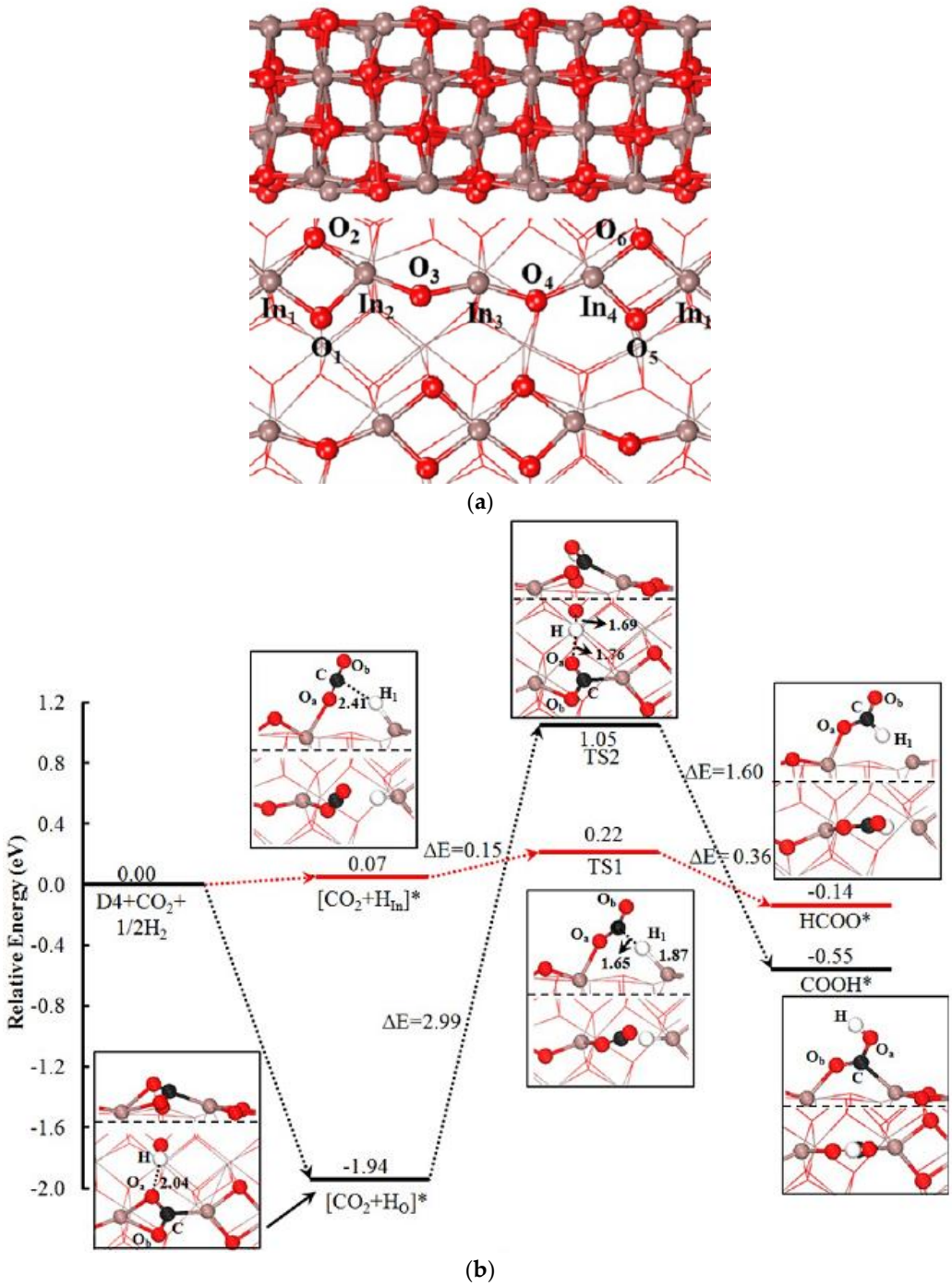

Figure 11. (**a**) Optimized structure of the In_2O_3 (110) surface. Red: O atoms; brown: In atoms. (**b**) Potential energy profiles of CO_2 hydrogenation and protonation on the D4 defective In_2O_3 (110) surfaces. Red line: hydrogenation; black line: protonation. A* represents the adsorption state of A on the surface, while [A+B]* represents the co-adsorption state of A and B on the surface, reproduced with permission from [47]. Copyright American Chemical Society, 2013.

Interestingly, Wang et al. synthesized a series of x% ZnO-ZrO_2 solid solution catalysts (x% represents the molar ratio of Zn) for CO_2 direct hydrogenation to CH_3OH [50]. Under the specified reaction conditions (5.0 MPa, H_2/CO_2 = 3:1 to 4:1, 593 K to 588 K), ZnO-ZrO_2 catalyst can achieve 86–91% methanol selectivity with single-pass CO_2 conversion more than 10%, better than the results reported by other researchers. Moreover, in the presence of 50 ppm SO_2 or H_2S in the reaction stream,

no deactivation was observed. Experimental results confirmed that ZrO_2 and ZnO alone showed little activity in methanol synthesis, while the catalytic performance was significantly enhanced and CO_2 conversion reached the maximum value when the Zn/(Zn + Zr) molar percentage is close to 13%. Demonstrated by CO_2-TPD, most of the CO_2 adsorbed on the Zr sites of ZnO-ZrO_2 catalyst, and the H_2-D_2 exchange experiment indicated that ZnO had much higher activity than ZrO_2. Therefore, in ZnO-ZrO_2 solid solution catalyst, the synergetic effect between the Zn and Zr sites markedly promotes the activation of H_2 and CO_2. To explain the reaction mechanism on the solid solution catalyst (ZnO-ZrO_2), in situ diffuse reflectance infrared Fourier transform spectroscopy (DRIFTS) and density functional theory (DFT) calculations were conducted. It was concluded that CO_2 direct hydrogenation to CH_3OH is dominated via the formate pathway, and CH_3OH was formed by H_3CO^* protonation on the surface of ZnO-ZrO_2 catalyst.

Although Cu-ZnO-based catalysts are highly selective for CO_2 conversion to methanol, there are still some serious problems during industrial operation, such as deactivation of active sites at high temperature and agglomeration of catalytic particles under industrial reaction conditions. To overcome these issues, researchers designed a series of bimetallic catalysts for the direct hydrogenation of CO_2 to CH_3OH. Jiang et al. prepared a series of Pd-Cu bimetallic catalysts supported on SiO_2 with a wide range of total metal loading (i.e., 2.4–18.7 wt %) and evaluated the catalytic performance for the reduction of CO_2 to CH_3OH. With a decrease in metal loadings, the CO_2 conversion dropped stepwise, namely from 6.6 to 3.7%. However, the CH_3OH STY was slightly enhanced by 31% from 0.16 to 0.21 mmol mol^{-1} s^{-1} [51]. To unclose the reaction mechanisms, the authors carried out in situ diffuse reflectance FT-IR (DRIFTS) measurements on Pd(0.34)-Cu/SiO_2 catalyst [52]. The resulting spectra identified that the dominant species on a bimetallic surface were formate and carbonyl species on a bimetallic surface, which were dependent on the catalyst composition. Therefore, they proposed that on Pd-Cu catalysts, the surface coverage of formate species was correlated to the methanol promotion, implying its vital role in CH_3OH synthesis. Bahruji et al. prepared PdZn/TiO_2 bimetallic catalysts by a solvent-free chemical vapor impregnation method [53]. According to the order in which the metals were impregnated, the catalysts could be classified as ^{2}Pd-^{1}Zn-TiO_2, ^{2}Zn-^{1}Pd-TiO_2, and PdZn/TiO_2 (1 and 2 represent the order of sequential metal impregnations). The experimental results showed that PdZn/TiO_2 catalyst achieved optimal catalytic performance, 10.1% CO_2 conversion and 40% CH_3OH selectivity. The formation of $ZnTiO_3$ and PdZn nanoparticles was confirmed via XPS, XRD, and TEM. Combining the experimental results, the authors proposed that PdZn nanoparticles were beneficial for methanol formation and catalytic stability. Although it is hard to assign the formation of the PdZn alloy to the differences between the preparation methods, an interaction between $Pd(acac)_2$ and $Zn(acac)_2$ precursors might be responsible for the production of the PdZn active site in terms of PdZn/TiO_2 catalyst. Additionally, Yin et al. reported the preparation of Pd@zeolitic imidazolate framework-8 (ZIF-8) catalyst for the conversion of CO_2 to CH_3OH [54]. The optimal methanol yield can reach 0.65 g g_{cat}^{-1} h^{-1} over a PdZn catalyst. As demonstrated by XPS, XRD, TEM and electron paramagnetic resonance (EPR), after H_2 reduction, PdZn alloy particles formed, and abundant oxygen defects existed on the ZnO surface. The experimental results revealed that the active site is a PdZn alloy rather than metallic Pd, in terms of CH_3OH formation.

Numerous studies suggested that promoters have an indispensable role in the catalytic performance of CuZn catalysts [55], although the mechanism of action still remains unclear. Pd-doped CuZn catalysts were prepared to evaluate the surface modification effect. An interesting observation was made from the volcano-shaped relationship between CH_3OH STY and Pd loading, which implied that an appropriate amount of Pd loading is beneficial for methanol synthesis. The chemisorption analyses further revealed a strong interaction between Pd and Cu surface, where a hydrogen spillover has taken place, generating more activated Cu sites. Hence, the CH_3OH STY and the methanol turnover frequency (TOF) improved a lot with Pd loading of 1 wt % [55]. In addition, a variety of bimetallic catalysts (e.g., Cu-Fe, Cu-Co, Cu-Ni, Co-Ga, Ni-Ga) have been evaluated by many researchers [56–59]. A possible catalytic reaction mechanism of CO_2 hydrogenation over Cu−Ni/CeO_2−NT is shown in

Figure 12. Details of the CO_2 conversion and product selectivity, along with reaction conditions of several representative catalytic systems are compared in Table 3. In terms of hydrogenation of CO_2 to CH_3OH, In-based and Pd-based catalysts have gradually drawn researchers' attention, besides traditional Cu-based catalysts. Additionally, many researchers demonstrated that 250 °C is the optimal temperature to produce CH_3OH with the high selectivity. According to the current experimental results, increasing the reaction pressure is also a good strategy to improve CO_2 conversion, but a high pressure means a high cost of operation and equipment.

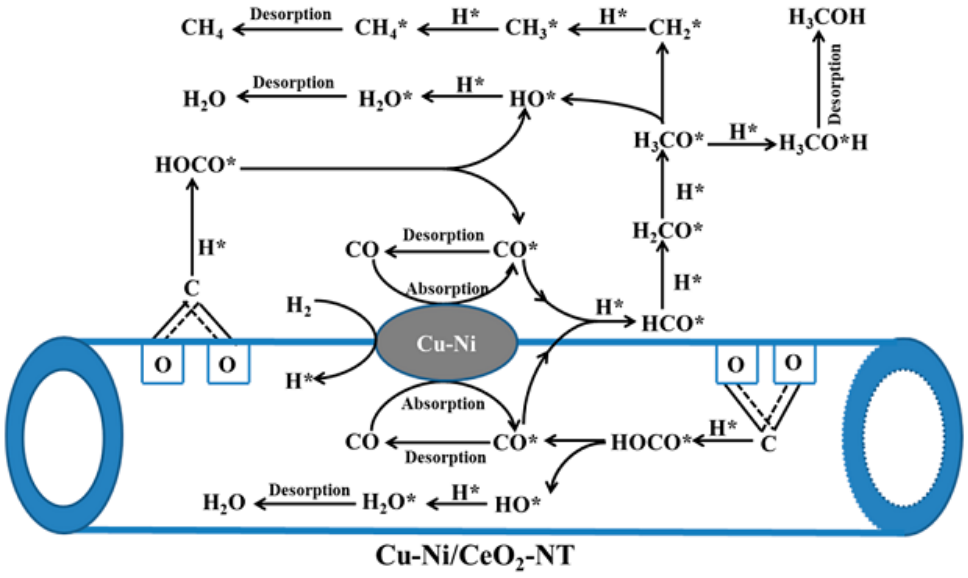

Figure 12. Possible catalytic mechanism of CO_2 hydrogenation over Cu−Ni/CeO_2−NT, reproduced with permission from [59]. Copyright American Chemical Society, 2018.

Table 3. Catalytic performance of several catalytic systems for CO_2 hydrogenation into CH_3OH, in terms of CO_2 conversion and CH_3OH selectivity, along with the reaction conditions.

Catalyst	H_2:CO_2	GHSV	Temperature (°C)	Pressure (MPa)	CO_2 Conversion (%)	CH_3OH Selectivity (%)
Cu-ZnO [42]	2.9	2160 [a]	250	3	29.2	83.6
Cu/g-C_3N_4-Zn/Al_2O_3 [44]	3	6800 [a]	250	1.2	~7.0	~55.0
CuO-ZnO-ZrO_2-GO [45]	3	15,600 [a]	240	2	N/A	75.8
W-Cu-Zn-Zr [46]	2.7	2400 [a]	240	3	19.7	49.3
In_2O_3 [48]	3	15,000 [a]	270	4	1.1	54.9
In_2O_3 [48]	3	15,000 [a]	330	4	7.1	3
In_2O_3 [49]	4	16,000–48,000 [b]	300	5	N/A	100
ZnO-ZrO_2 [50]	3-4	24,000 [a]	315-320	5	>10	86–91
Pd-Zn-TiO_2 [53]	3	916 [b]	250	2	10.3	61
Pd-Zn-ZIF-8 [54]	3	21,600 [a]	270	4.5	~22.0	~50.0
Pd-Cu-Zn [55]	3	10,800 [a]	270	4.5	~8.0	~65.0
Co_5Ga_3 [58]	3	N/A	250	3	1	63
$CuNi_2$/CeO_2-NT [59]	3	6000 [b]	260	3	17.8	78.8
Cu-Zn-SiO_2 [60]	3	2000 [a]	220	3	14.1	57.3
Ni_5Ga_3/SiO_2/Al_2O_3/Al [61]	3	3000 [a]	210	0.1	~1.0	86.7
Cu-Zr-SiO_2 [62]	3	N/A	230	5	N/A	77
Cu/Mg/Al [63]	2.8	2000 [b]	200	2	3.6	31
Cu-Ce-Zr [64]	3	7500 [a]	250	3	14.3	53.8
Cu-TiO_2 [65]	3	3600 [a]	260	3	N/A	64.7
Cu-Zn-Mn-KIT-6 [66]	3	120,000 [a]	180	4	8.2	>99.0
Cu-SBA-15 [67]	3	N/A	210	2.2	13.9	91.3
Au-CuO/SBA-15 [68]	3	3600 [b]	250	3	24.2	13.5
Cu-Zr-SBA-15 [69]	3	N/A	250	3.3	15	N/A
Pd/In_2O_3 [70]	4	>21,000 [a]	300	5	>20.0	>70.0

[a] mL g_{cat}^{-1} h^{-1}; [b] h^{-1}; N/A: not available.

2.4. CO_2 to Other Products

Besides CO, CH_4, and CH_3OH, dimethyl ether (DME), light olefins [71–74], alcohol [75], isoparaffins [76], and aromatics [77,78] have also been produced by CO_2 hydrogenation. Clearly, in terms of CO_2 conversion, the coupling of C-C bond to produce higher hydrocarbons and oxygenates is a technological barrier. However, taking advantage of tandem catalysis to realize one-step synthesis of hydrocarbons via hydrogenation of CO_2 is feasible. The extensive studies can be mainly categorized into two categories: methanol-mediated and non-methanol-mediated reactions [79,80]. In the methanol-mediated approach, DME is usually produced as main product, while for the non-methanol-mediated approach, alkenes and alkanes are generally produced as main products. The possible reaction mechanism for CO_2 hydrogenation to DME and light olefins is shown in Scheme 4.

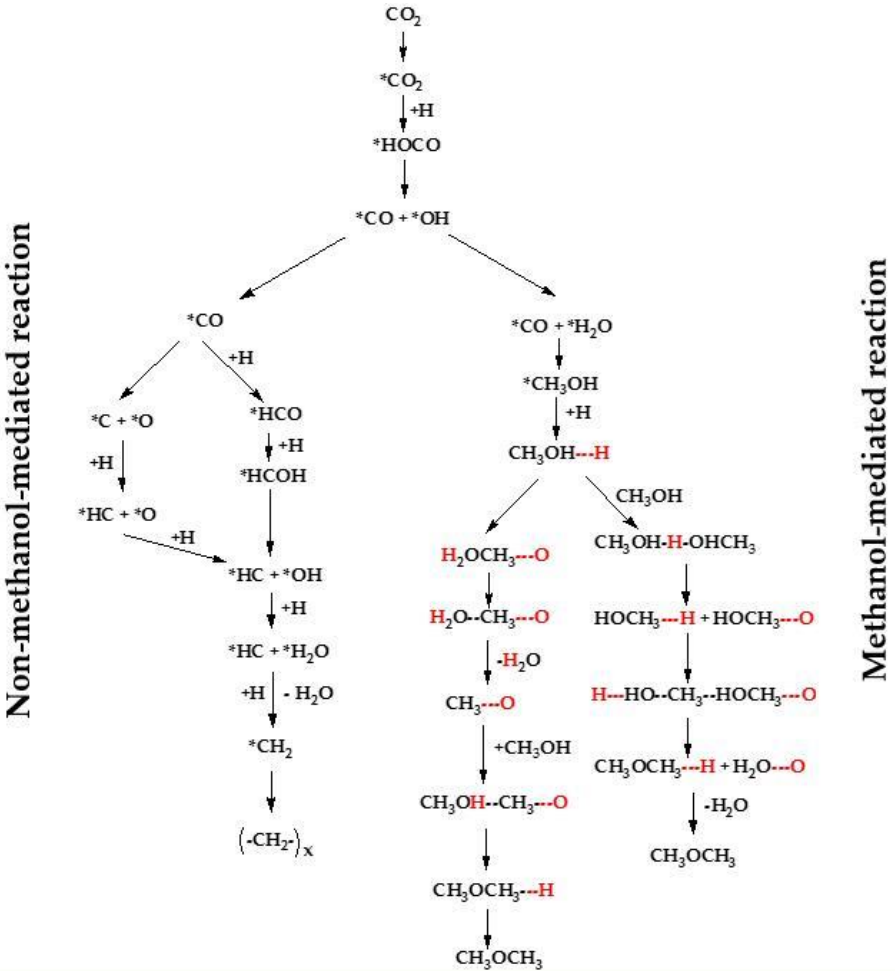

Scheme 4. Possible reaction pathways for CO_2 hydrogenation to DME and light olefins. Note: ---H, ---O derived from H-ZSM5 zeolite, reprinted with permission from [21]. Copyright Elsevier, 2016.

Cu-based catalysts are in practice used for methanol synthesis, and HZSM-5 zeolites are widely employed for methanol dehydration due to its solid acid catalysis. Therefore, a variety of studies have been reported with regard to the bi-functional catalysts consisting of Cu and HZSM-5 used for the direct hydrogenation of CO_2.

Zhang et al. reported a Cu-ZrO_2/HZSM-5 catalyst promoted by Pd/CNT for direct synthesis of DME from CO_2/H_2 [79]. Although a minor amount of the Pd-decorated CNTs into the CuZr/HZSM-5 catalytic system caused little change in the activation energy for CO_2 conversion compared with the CuZr/HZSM-5 catalyst, the former created a micro-environment including higher concentration of active H species and adsorbed CO_2 species on the surface of the catalyst system. Owing to the increase

of hydrogenation reactions, under reaction conditions of 5 MPa and 523 K, the specific rate of CO_2 hydrogenation-conversion was 1.22 times higher than the pure CuZr/HZSM-5 catalyst. Furthermore, Zhang et al. reported a series of V-modified CuO-ZnO-ZrO_2/HZSM-5 catalysts which were prepared via an oxalate co-precipitation method for the synthesis of DME from CO_2/H_2 [81]. The catalytic performances of the catalysts were strongly dependent on the content of V, which was confirmed by XRD, N_2O chemisorption, and X-ray photoelectron spectroscopy (XPS). Similarly, the influence of the promoter—i.e., La and W—has also been examined. The optimal catalytic activity was obtained (43.8% CO_2 conversion and 71.2% DME selectivity) when the amount of La was 2 wt %. In contrast, the Cu-ZnO-ZrO_2 catalyst admixed with WO_x obtained 18.9% CO_2 conversion and 15.3% DME selectivity. Obviously, La is a better promoter compared with W, and this can be explained by the fact that the reducibility and dispersion of bi-functional catalysts (CuO-ZnO-Al_2O_3-La_2O_3/HZSM-5) were largely dependent on the modification of La, while the hybrid catalyst (Cu-ZnO-ZrO_2-WO_x/Al_2O_3) modified by W strongly adsorbed water molecules, resulting in a lower catalytic performance. Moreover, as shown in Figure 13, the STY of DME of different WO_x/Al_2O_3 catalysts (i.e., on supports with different pore sizes) as a function of W surface density shows a volcanic curve relation. Details of CO_2 conversion and DME selectivity reported recently are shown in Table 4 [82,83]. The above studies indicate that the current catalysts used for DME preparation from CO_2/H_2 are still dominated by Cu-based-HZSM-5 catalysts. Some other zeolite catalysts (SBA-15, SAPO-5, SUZ-4) with similar acid properties (acid content and acid strength) as HZSM-5 zeolite may be a direction of future research.

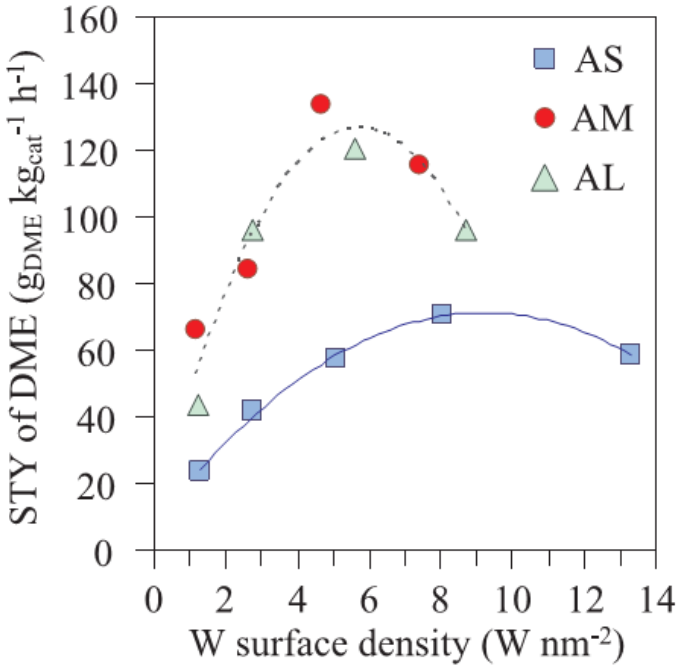

Figure 13. STY of DME of different WO_x/Al_2O_3 catalysts, with different support pore size as a function of W surface density. AS, AM, and AL refer to the mean pore size of alumina supports with small, medium and large pores, respectively, reproduced with permission from [83]. Copyright Elsevier, 2018.

Among the large-scale technologies with industrial potential, the conversion of CO_2 to DME is promising and relatively mature [84]. Korea Gas Corporation (KOGAS) has developed a DME plant, with CO_2 as a raw material. The schematic diagram of the KOGAS tri-reforming process is shown in Figure 14 [85,86]. Kansai Electric Power Co. and Mitsubishi Heavy Industries have realized a bench-scale (100 cm^3 catalyst loading) experiment for DME synthesis [87,88]. However, during the reaction process, water formation decreased the yield of DME [89–91]. Catizzone et al. and Bonura et al. evidenced that zeolites or ferrierite could effectively mitigate the influence of water and avoid catalyst sintering [89,90]. In a fixed bed reactor, kinetic modeling confirmed the negative

effect of water (formed during the reaction process) on DME production, which is consistent with the experimental results. Therefore, Falco et al. suggested that hydrophilic membranes could be promising for industrial production of DME [92]. Recently, Fang et al. advocated CO_2 capture and conversion by using a membrane reactor system, where a high-temperature mixed electronic and carbonate-ion conductor (MECC) membrane was used for CO_2 capture and a solid oxide electrolysis cell (SOEC) was used for CO_2 reduction [93]. Furthermore, based on membrane technology, Sofia et al. carried out a techno-economic analysis project of power and hydrogen co-production via an integrated gasification combined cycle (IGCC) plant with CO_2 capture [94]. The development of membrane technology would be an advantageous factor for the capture and utilization of CO_2.

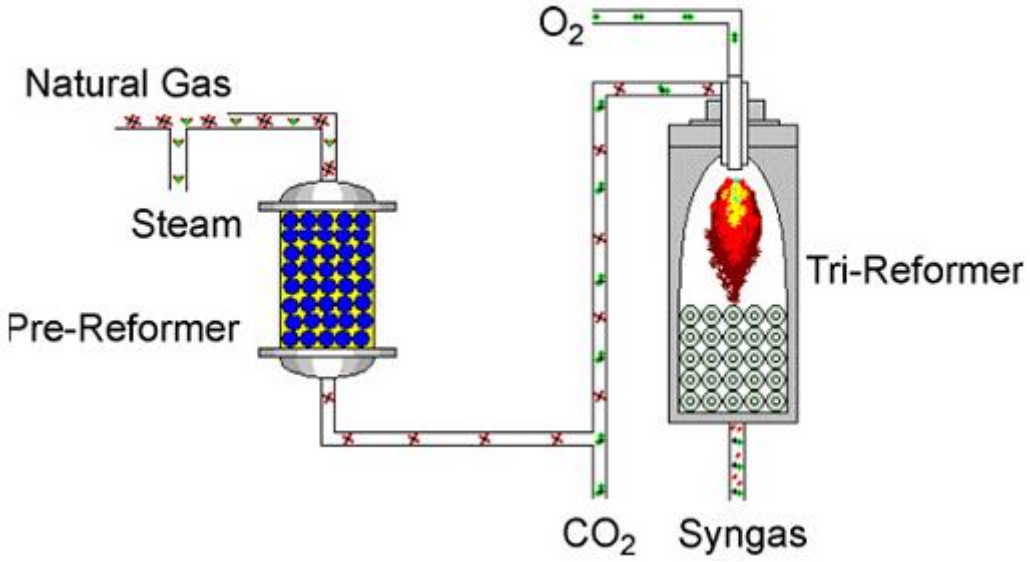

Figure 14. Schematic diagram of KOGAS tri-reforming process, reproduced with permission from [86]. Copyright Elsevier, 2009.

Li et al. synthesized a novel ZnZrO/SAPO tandem catalyst, combined by a ZnO-ZrO_2 solid solution and a Zn-modified SAPO-34 zeolite, which achieved 80–90% olefin selectivity among the hydrocarbon products [95]. Based on the surface reaction kinetics, they proposed that the tandem reaction process proceeded as follows: (1) generation of CH_xO species on ZnZrO via CO_2 reduction; (2) olefins production from the derived CH_xO species which migrate/transfer onto SAPO zeolite pore structure. Moreover, experimental results confirmed that the excellent selectivity can be ascribed to the effective synergy between ZnZrO and SAPO for the tandem catalyst. In addition, this catalyst (ZnZrO and SAPO-34) shows an excellent stability toward thermal and sulfur treatments, indicating the potential value for industrial application.

Recently, CO_2 was converted to aromatics with a selectivity up to 73%, at 14% CO_2 conversion over ZnZrO/HZSM-5 catalyst [77]. Demonstrated by operando infrared (IR) characterization, Li et al. proposed that CH_xO, as an intermediate species, transformed from the ZnZrO surface into the pore structure of HZSM-5, which is responsible for C-C bond formation for aromatics production. The reaction scheme is shown in Figure 15. Interestingly, the presence of H_2O and CO_2 markedly suppressed the generation of polycyclic aromatics, consequently, enhanced the stability (100 h in the reaction stream) of the tandem catalyst, which showed potential industrial application prospects. Similarly, Ni et al. synthesized a tandem catalyst of $ZnAlO_x$ and HZSM-5, which yields 73.9% aromatics selectivity and 0.4% CH_4 selectivity among the carbon products without CO [78]. Confirmed by XRD, SEM, TEM, and element distribution analysis, ZnAlOx was formed and uniformly dispersed in the tandem catalyst. Furthermore, demonstrated by 2,6-di-tert-butyl-pyridine absorption (DTBPy-FTIR), the external Brønsted acid of HZSM-5 can be shielded by $ZnAlO_x$, which is beneficial to aromatization. According to the operando diffuse reflectance infrared Fourier transform spectroscopy (DRIFTS)

study, they proposed the following possible reaction mechanism: MeOH and DME, produced by hydrogenation of formate species, are transmitted to HZSM-5 and then converted into olefins and finally aromatics.

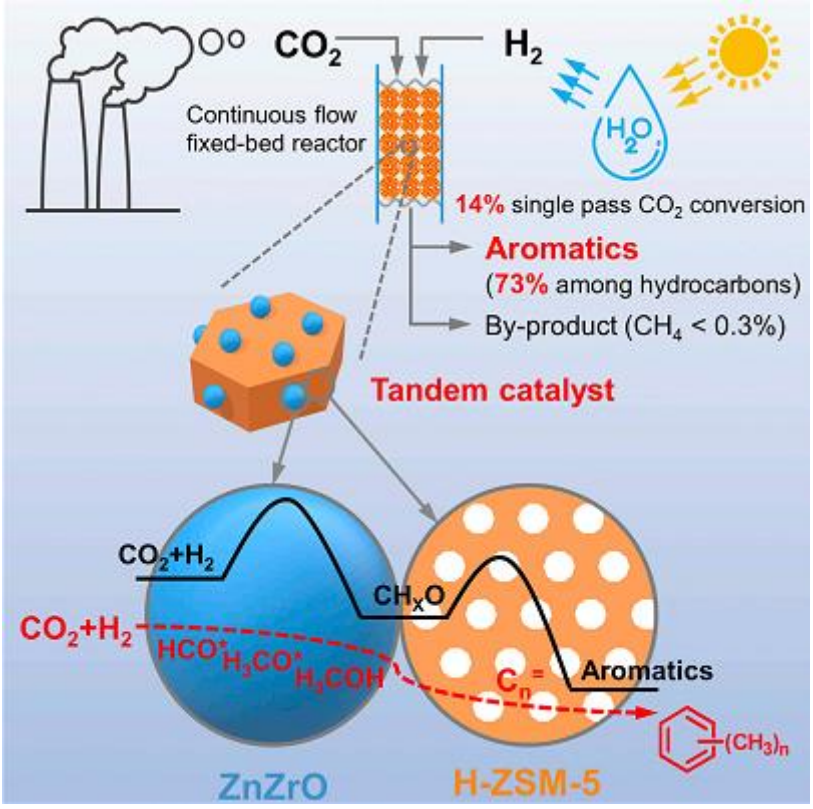

Figure 15. Reaction scheme of CO_2 hydrogenation to aromatics, reproduced with permission from [77]. Copyright Elsevier, 2019.

Non-methanol-mediated reactions, i.e., the direct hydrogenation of CO_2 to light olefins is even more significant than CH_3OH synthesis from CO_2 hydrogenation, since a large proportion of methanol is used for the synthesis of olefins in industry, through the methanol-to-olefins (MTO) reaction by using SAPO-34 zeolite catalysts. CO_2 to lower olefins can be realized by coupling of the RWGS reaction and F–T synthesis, as shown in Schemes 1 and 3.

Iron-based catalysts has been considered as an excellent option for the synthesis of light olefins from CO_2/H_2, mainly because of their excellent activity, high selectivity, and low price. Using honeycomb-structure graphene (HSG) as the support and K as a promoter, Wu et al. prepared an iron-based catalyst [80]. They found out that the confinement effect of the porous HSG was beneficial for the sintering of the Fe active sites, and within 120 h stability test, no significant deactivation occurred. In addition, as confirmed by CO_2 temperature programmed desorption (CO_2-TPD) and H_2-TPD, they found out that potassium as a promoter effectively enhanced the chemisorption and activation of the reactants CO_2 and H_2. Moreover, as revealed by ^{57}Fe Mossbauer absorption spectroscopy, for the Fe/HSG catalyst, there were two doublets with isomer shift (IS) of 0.96 mm s^{-1} and quadrupole splitting (QS) of 0.28 mm s^{-1} and IS of 1.21 mm s^{-1} and QS of 1.82 mm s^{-1}, which corresponded to the Fe (II) species in low- and high-coordination environments. Instead, for the FeK1.5/HSG catalyst, only one doublet with IS of 0.31 mm s^{-1} and QS of 1.05 mm s^{-1} ascribed to the Fe (III) species, which implies that K is capable of stabilizing high valence-state iron (Fe (III)) during CO_2 hydrogenation to light olefins (CO_2–FTO). The above mentioned three factors contributed to the excellent catalytic performance, i.e., 56% olefins selectivity and a 120-h stability testing experiment (as shown in Figure 16).

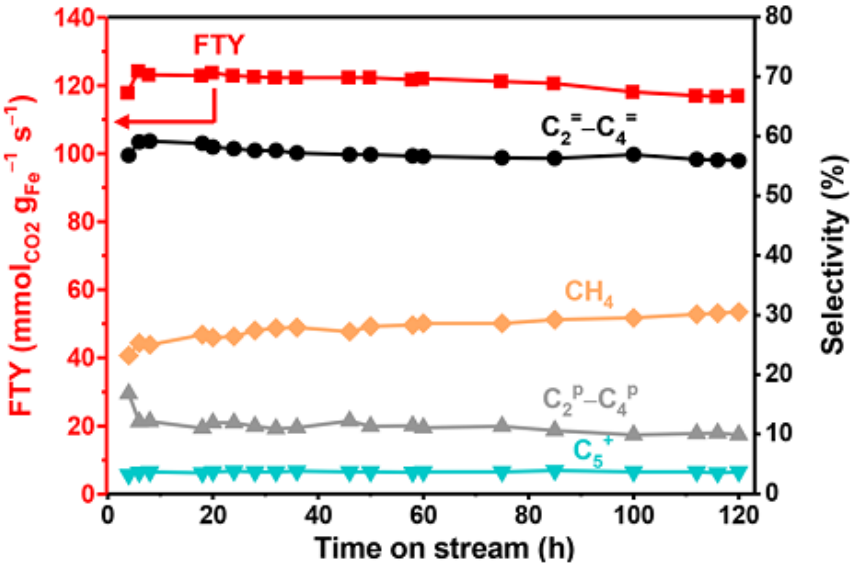

Figure 16. CO_2−FTO results over the FeK1.5/HSG catalyst during 120 h on stream (Fe time yield to hydrocarbons, termed as FTY). Reaction conditions: 0.15 g catalyst, T = 613 K, P = 20 bar, H_2/CO_2 = 3 by volume, and the space velocity of 26 L h^{-1} g^{-1}. The CO selectivity is in the range of 39−43%, reproduced with permission from [80]. Copyright American Chemical Society, 2018.

Zhang et al. used an impregnation method to prepare Fe-Zn-K catalysts, in which K was used as a promoter [71]. The experimental results showed that the Fe-Zn-K catalyst with H_2/CO reduction showed the best catalytic activity, with 51.03% CO_2 conversion and 53.58% C_2–C_4 olefins selectivity, at the reaction conditions of 593 K and 0.5 MPa. XRD, H_2-TPR, and XPS characterization results revealed that, in the Fe-Zn-K catalyst, $ZnFe_2O_4$ spinel phase and ZnO phase were formed. Among them, $ZnFe_2O_4$ spinel phase strengthens the interaction between iron and zinc, and changed the reduction and CO_2 adsorption behaviors. In addition, the H_2-TPR profiles show that the catalyst modified by K contributed to a slight shift of the initial reduction peak to higher temperature, indicating the reduction of Fe_2O_3 and formation of Fe phase was inhibited by K modification.

You et al. investigated the catalytic activity of non-supported Fe catalysts (bulk Fe catalysts) modified by alkali metal ions (i.e., Li, Na, K, Rb, Cs) for the conversion of CO_2 to light olefins [72]. By calcining ammonium ferric citrate, non-supported Fe catalyst was prepared. Compared with Fe catalyst without modification (5.6% CO_2 conversion, 0% olefins), the modification of the Fe catalyst with an alkali metal ion markedly enhanced the catalytic activity for CO_2 conversion to light olefins. For Fe catalyst modified by K and Rb, the conversion of CO_2 and the olefin selectivity (based on only the hydrocarbon compounds, without CO) increased to about 40% and 50%, respectively, and the yield of light (C_2–C_4) olefins can reach 10–12%. Further investigation via XRD showed that over the alkali-metal-ion-modified Fe catalysts, Fe_5C_2 was formed, while in the unmodified catalyst, iron carbide species were not observed after the reaction. Accordingly, they proposed that in the presence of an alkali metal ion, the generation of iron carbide species was one possible reason for the enhanced catalytic activity. Therefore, modification by alkali metal ions remains a good strategy to tune the product distribution.

Additionally, Wei et al. reported a highly efficient, stable and multifunctional Na–Fe_3O_4/HZSM-5 catalytic system [76], for direct hydrogenation of CO_2 to gasoline-range (C_5–C_{11}), in which the selectivity of C_5–C_{11} hydrocarbons reached 78% (based on total hydrocarbons), while under industrial conditions only reached 4% methane selectivity at a 22% CO_2 conversion. Characterization by high resolution transmission electron microscopy (HRTEM), X-ray diffraction (XRD), and Mossbauer spectroscopy showed that two different types of iron phase—i.e., Fe_3O_4 and x-Fe_5C_2—were discerned in the spent Na–Fe_3O_4 catalyst, which cooperatively catalyzed a tandem reaction (RWGS and FT).

The possible reaction scheme for CO_2 hydrogenation to gasoline-range hydrocarbons is shown in Figure 17. Furthermore, acid sites existing in the HZSM-5 zeolite were favorable for acid-catalyzed reactions (oligomerization, isomerization, and aromatization). Notably, the multifunctional catalyst exhibited a significant stability for 1000 h on stream, showing the potential as promising industrial catalyst material for CO_2 conversion to liquid fuels. Similarly, Gao et al. investigated a bi-functional catalytic system composed of In_2O_3 and HZSM-5, which can achieve 78.6% C_{5+} selectivity with only 1% CH_4 at a 13.1% CO_2 conversion [73]. As demonstrated by Ye et al. [47], CO_2 and H_2 can be activated in the oxygen vacancies on the In_2O_3 surfaces, and catalyzed CH_3OH formation. Subsequently, C−C coupling occurred inside the zeolite pores structure (HZSM-5) to synthesize gasoline-range hydrocarbons with a relatively high octane number (C_{5+}).

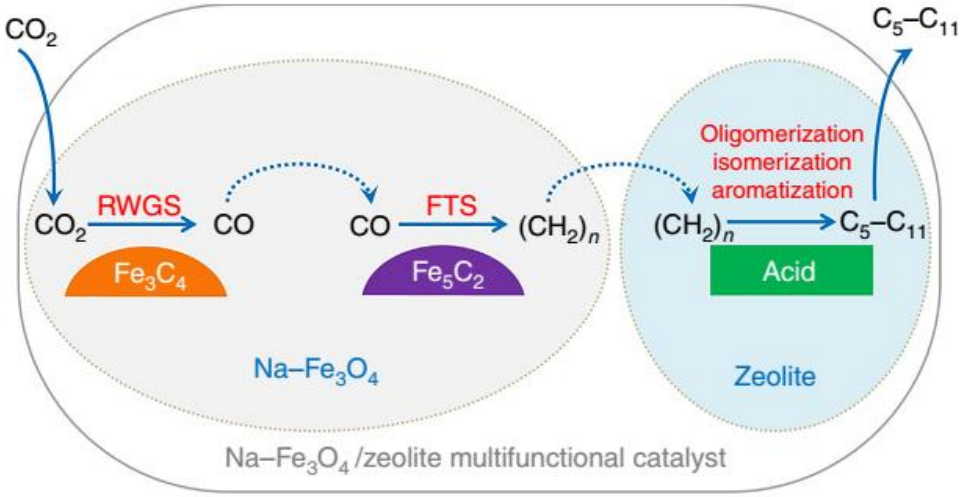

Figure 17. Reaction scheme for CO_2 hydrogenation to gasoline-range hydrocarbons, reproduced with permission from [76]. Copyright Nature Publishing Group, 2017.

Details of the conversion and selectivity for the hydrogenation of CO_2 into other products, along with the reaction conditions of several representative catalytic systems, are compared in Table 4. Fe-based catalysts are beneficial for the production of olefins, while Cu-based + HZSM-5 is still a dominant catalytic system for CO_2 conversion to DME. Similarly, 250 °C is the optimal temperature for the production of DME based on the current experimental results, and 300–400 °C, which is close to industrial production conditions, seems to be better for the direct conversion of CO_2 to olefins. On the other hand, the selectivity of DME can be maintained upon increasing GHSV (>10,000 mL g_{cat}^{-1} h^{-1}), but the high selectivity of olefins generally relies on a relatively low GHSV (<5000 mL g_{cat}^{-1} h^{-1}).

Table 4. Catalytic activity of several catalysts for CO_2 hydrogenation into other products (e.g., DME, olefins, alcohol, isoparaffins, gasoline, aromatics), in terms of CO_2 conversion and product selectivity, along with the reaction conditions.

Catalyst	H_2:CO_2	GHSV	Temperature (°C)	Pressure (MPa)	CO_2 Conversion (%)	Selectivity (%)
Fe-Zn-K [71]	3	1000 [b]	320	0.5	51.03	olefins (53.58)
K-Fe [72]	3	1200 [a]	340	2	38	light olefins (78)
In/HZSM-5 [73]	3	9000 [a]	340	3	13.1	liquid fuels (78.6)
Ce-Pt@mSi-Co [74]	3	N/A	250	N/A	~3.0	C_2–C_4 (60)
K/Cu-Zn-Fe [75]	3	5000 [b]	300	6	42.3	alcohol (56.43)
Na-Fe/HMCM-22 [76]	2	4000 [a]	320	3	26	isoparaffins (74)
ZnZrO-HZSM-5 [77]	N/A	1200 [a]	320	4	14	aromatic (73)
ZnAlOx-HZSM-5 [78]	3	2000 [a]	320	3	9.1	aromatics (74)
Cu-Zr-Pd/HZSM-5 [79]	3	25,000 [a]	250	5	18.9	DME (51.8)
Fe-K/HSG [80]	3	26,000 [a]	340	20	N/A	olefins (59)

Table 4. *Cont.*

Catalyst	H_2:CO_2	GHSV	Temperature (°C)	Pressure (MPa)	CO_2 Conversion (%)	Selectivity (%)
V-Cu-Zn-Zr/HZSM-5 [81]	3	4200 [b]	270	3	32.5	DME (58.8)
Cu-Zn-Al-La/HZSM-5 [82]	3	3000 [b]	250	3	43.8	DME (71.2)
ZnO-ZrO_2-SAPO-34 [95]	N/A	3600 [a]	380	2	12.6	olefins (80–90)
Cu-ZnO-Al_2O_3 [96]	3	10 [b]	270	5	9	DME (31)
In-Zr/SAPO-34 [97]	3	9000 [a]	380	3	26.2	C_{2+} (36.1)
Cu-Zn-kaolin-SAPO-34 [98]	3	1800 [a]	400	3	50.4	C_2–C_4 (65.3)
Fe/C-Bio [99]	3	N/A	320	1	31	$C_{4–18}$ alkenes (50.3)
Cu-Zn-Zr/HZSM-5 [100]	3	10,000 [a]	220	3	9.6	DME (46.6)
Cu-Zn-Zr/HZSM-5 [101]	3	9000 [a]	240	3	~30	DME (~35)
Cu-Zn-Al/HZSM-5 [102]	3	4200 [b]	270	3	30.6	DME (49.02)
Cu-Zn-Al/HZSM-5 [103]	3	1800 [a]	262	3	46.2	DME (45.2)
Cu-Zn-Zr-zeolite [104]	3	10,000 [b]	240	3	24	DME (38.5)
Cu-Zn-Al/HZSM-5 [105]	3	1800 [a]	270	3	48.3	DME (48.5)
Fe-K/HPCMs-1 [106]	3	3600 [a]	400	3	33.4	olefins (47.6)
Na-Fe/HZSM-5 [107]	3	4000 [a]	320	3	22	C_5–C_{11} (78)
Fe_5C_2-/a-Al_2O_3 [108]	3	3600 [a]	400	3	31.5	C_{2+} (69.2)
Fe-Zr-Ce-K [109]	3	1000 [b]	320	2	57.34	C_2–C_4 (55.67)
Fe/C+K [110]	3	24,000 [a]	320	30	24	C_2–C_6 (36)
Co-Cu/TiO_2 [111]	3	3000 [a]	250	3	18.4	C_{5+} (42.1)

[a] mL g_{cat}^{-1} h^{-1}; [b] h^{-1}; N/A: not available.

2.5. Opportunities of Heterogeneous Catalysis for CO_2 Conversion

The relationship between products selectivity and CO_2 conversion by heterogeneous catalytic hydrogenation is shown in Figure 18. It is obvious that, in the RWGS reaction, although the CO selectivity reaches up to nearly 100%, the CO_2 conversion is low. In the methanation reaction of CO_2, the CH_4 selectivity is high enough, and the CO_2 conversion also exceeds 50%. With regard to the synthesis of CH_3OH, DME, and light olefins, the relationship between conversion and selectivity is less clear.

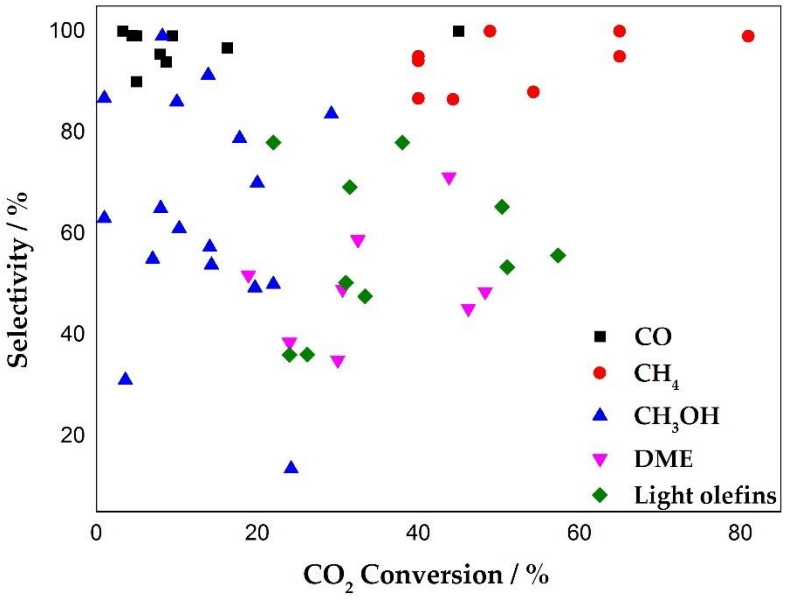

Figure 18. Selectivity and conversion distribution of different products according to recent reports in heterogeneous catalysis.

In the RWGS reaction, CO is mainly produced over Fe-, Co-, Mo-, and Pt-based catalysts (Table 1), while CO_2 methanation is typically carried out on Co- and Ni-based catalysts (Table 2). Although CO is a main component of syngas and CH_4 is an important energy resource, neither is the best product for CO_2 conversion from a relatively economic point of view. Furthermore, the conversion and utilization of CO and CH_4 is also an important research field, which also implies that CO and CH_4 are not the

optimal choice as end-products of CO_2 conversion. Therefore, the coupling reaction is a potential direction for CO_2 conversion to some higher value products, i.e., CH_3OH and light olefins.

Cu-ZnO-based catalyst is still the main catalytic material for direct conversion of CO_2 to CH_3OH under industrial reaction condition, while highly innovative methodologies are awaited to achieve low-pressure and low-temperature CH_3OH synthesis processes. Considering the industrial application value of methanol, exploring novel catalytic systems and designing rational reactors to improve the catalytic activity should be targeted in the future. DME, up to now, is synthesized via Cu-based and H-ZSM5 catalyst (Table 4), and this process essentially remains a two-step tandem reaction. Hence, the bottleneck of DME production could be the deactivation of CH_3OH dehydration catalyst, due to water poisoning. The formation of coke is also the major reason of catalyst deactivation, especially in a relatively long-term operation process. To maintain high activity of catalyst for the production of DME, water- and coke-resistant catalysts need to be developed for CH_3OH dehydration.

As shown in Table 4, the direct hydrogenation of CO_2 to light olefins is mainly catalyzed by Fe-based catalysts. However, the starting point of current research work is mainly the coupling of RWGS, F–T and/or methanol-to-olefins (MTO) reactions. Therefore, suitable catalytic materials are sought for the coupling of C-C bonds, which is an effective strategy for improving the catalytic activity.

3. Plasma Catalysis

Plasma, the 'fourth state of matter', consists of electrons, neutral species (i.e., molecules, radicals, and excited species) and ions. Plasma can be in so-called thermal equilibrium or not, based on which it is subdivided into 'thermal plasma' and 'non-thermal plasma' (NTP) [13,112,113]. In non-thermal plasma, the gas temperature remains near room temperature, while electrons temperature is extremely high, usually in the range of 1–10 eV (~10,000–100,000 K). The latter is enough to activate stable gas molecules into reactive species (e.g., radicals, excited atoms, molecules, and ions). These reactive species, especially the radicals, can trigger reactions at low temperature. That is, NTP offers a unique approach to enable thermodynamically unfavorable chemical reactions to proceed at low temperature by breaking thermodynamic limits. Nevertheless, the control of selectivity of desired products in plasma is extremely difficult, since the reactions in plasma are mainly triggered through nonselective collision between active species (radicals, molecules, atoms, and ions).

To improve the desired product selectivity of the reactions in plasma, the combination of catalysts with plasma technology (so-called plasma catalysis) is a promising strategy, since catalysts usually have a special feature of regulating product distribution.

NTP can be generated through various types of discharges—i.e., microwave discharges, glow discharges, gliding arc discharges, dielectric barrier discharges (DBD), etc.—but DBD are the best option to be used in plasma catalysis. Indeed, DBDs are usually operated at atmospheric pressure and ambient temperature, and the integration of DBD plasma with catalysts has the advantages of simple operation and low cost. Thus plasma-driven direct hydrogenation of CO_2 is mostly based on DBD plasmas. The possible plasma/catalyst synergism is illustrated in Figure 19 [13].

A lot of research has been performed for pure CO_2 splitting, in various types of plasma reactors, including DBD, microwave discharge and gliding arc discharge, without catalysts [114–117]. A typical experimental set-up of a DBD plasma for CO_2 decomposition is shown in Figure 20. Paulussen et al. studied the conversion of CO_2 to CO and oxygen in DBD [114], and they found that the gas flow rate is the most crucial parameter affecting the CO_2 conversion. At 0.05 L min^{-1} flow rate, 14.75 W cm^{-3} power density and 60 kHz discharge frequency, 30% CO_2 conversion was achieved. The performance might be further enhanced by optimizing the discharge parameters (i.e., power, frequency, dielectric material) or by implementing parallel reactors.

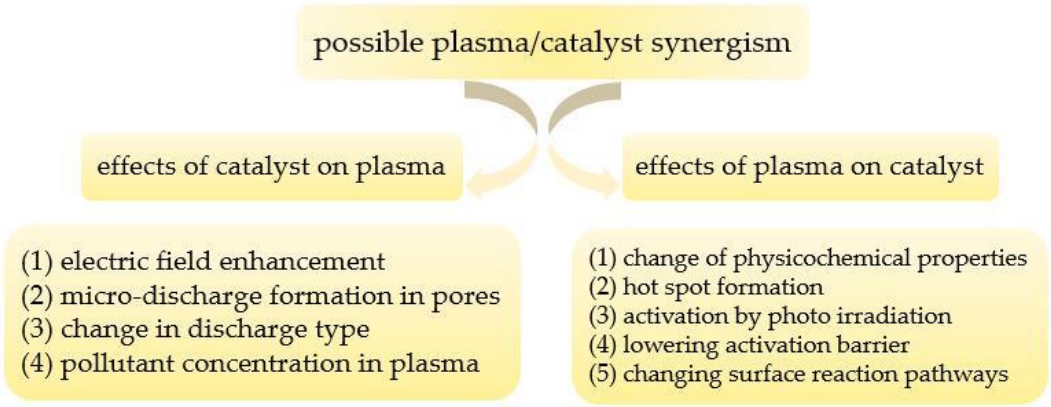

Figure 19. Overview of the possible effects of the catalyst on the plasma and vice versa, possibly leading to synergism in plasma-catalysis, reproduced with permission from [13]. Copyright Royal Society of Chemistry, 2017.

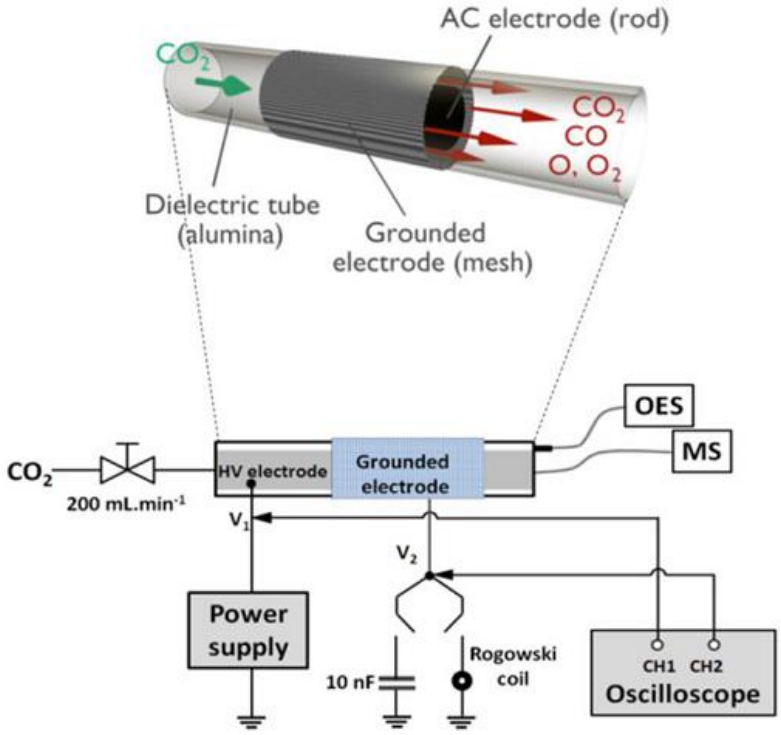

Figure 20. Schematic diagram of the experimental set-up used in the decomposition of CO_2, reproduced with permission from [116]. Copyright IOP Publishing, 2016.

Dry reforming of methane (DRM), i.e., the combined conversion of CH_4 and CO_2 by plasma and/or plasma catalysis, has attracted extensive attention in recent years. For instance, Li et al. studied CO_2 reforming of CH_4 by taking advantage of atmospheric pressure glow discharge plasma [118]. Liu et al. reported high-efficient conversion of CO_2 and CH_4 in AC-pulsed tornado gliding arc plasma [119]. Kolb et al. investigated DRM in a DBD reactor [120]. In the above-mentioned studies [118–120], syngas (CO and H_2) was produced as the main product. Recently, Wang et al. reported a novel one-step reforming of CO_2 and CH_4 into liquid oxygenate products, dominated by acetic acid, at room temperature by the coupling of DBD plasma and catalysts [121]. They examined the effect of CH_4/CO_2 molar ratio and of various catalysts (γ-Al_2O_3, Cu-γ-Al_2O_3, Au-γ-Al_2O_3, Pt-γ-Al_2O_3). Interestingly, compared with plasma-only mode, the coupling of plasma and catalysts

tuned the selectivity of liquid chemicals, and oxygenates selectivity was achieved up to approximately 60% when Cu catalyst was used. Details about the effects of operating mode and catalysts on the CO_2 conversion reaction results are shown in Figure 21. Although much efforts need to be made to reveal the unknown mechanisms, the results are attractive and show an excellent application prospect.

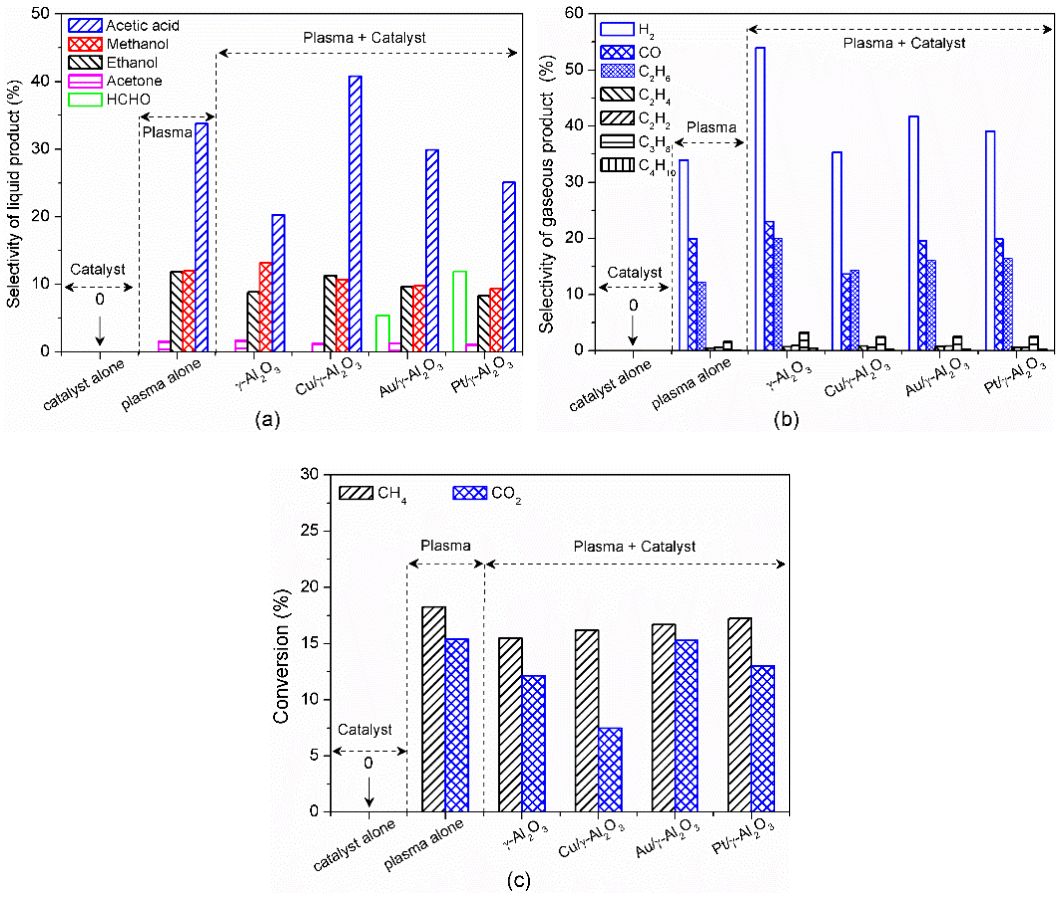

Figure 21. Effect of operating modes and catalysts on the reaction: (**a**) selectivity of liquid oxygenates, (**b**) selectivity of gaseous products, (**c**) conversion of CH_4 and CO_2 (total flow rate 40 mL min^{-1}, discharge power 10 W, catalyst ca. 2 g), reproduced with permission from [121]. Copyright Wiley online library, 2017.

Besides the above-mentioned metal catalysts, zeolites have also been used in plasma catalytic DRM. Zhang et al. studied the catalytic performance of zeolite catalysts (i.e., NaA, NaY, and HY) for the direct conversion of CH_4 and CO_2 at relatively low temperature range and ambient pressure via DBD plasma [122], and the products were dominated by syngas and C_4 hydrocarbons. Form the investigated catalysts (NaA, NaY, and HY), HY zeolite catalyst exhibited the best performance (26.7% CO_2 conversion and 52.1% C_4 hydrocarbon selectivity), which was mainly attributed to the appropriate pore size and electrostatic properties of HY zeolite.

Although direct hydrogenation of CO_2 to CH_3OH is an exothermic reaction, studies of heterogeneous catalysis for CO_2 hydrogenation to CH_3OH were usually operated at high temperature and high pressure, mainly caused by the high stability of CO_2 and the low equilibrium constant at atmospheric pressure. Plasma catalysis, however, is a promising approach to enable CO_2 conversion to CH_3OH at ambient conditions, and has gradually attracted more and more interest. For instance, Eliasson et al. reported the direct hydrogenation of CO_2 to CH_3OH by coupling of DBD plasma and a discharge-activated catalyst (CuO-ZnO-Al_2O_3) [123]. By comparison of the experiments, with catalyst only, discharge only, and discharge + catalyst, they found that DBD plasma effectively lowered the

optimal reaction temperature corresponding to the best catalytic performance. Indeed, the optimal reaction temperature was 493 K for catalyst only, while in terms of discharge only and discharge + catalyst, the optimal reaction temperature for CO_2 conversion was 373 K. The maximum selectivity for the methanol formation (10%) was achieved at a temperature of 373 K, which implies that the plasma improved the catalytic activity of CuO-ZnO-Al_2O_3 catalyst at low temperature. Additionally, the authors found that low input power and high pressure are beneficial for the improvement of the methanol selectivity.

Zeng et al. studied CO_2 hydrogenation by combining various catalysts (i.e., Cu/γ-Al_2O_3, Mn/γ-Al_2O_3, and Cu–Mn/γ-Al_2O_3) with DBD plasma in a coaxial packed-bed [124]. The experimental results showed that the addition of catalysts in the reactor improved the conversion of CO_2. At the same time, with the increase of the H_2/CO_2 molar ratio, the CO_2 conversion was improved, and the CO yield was also enhanced. It is also worth mentioning that, compared with plasma only experiments, the energy efficiency was enhanced by adding catalysts, although the synergetic mechanism between catalysts and plasma is still unknown.

Recently, Wang et al. examined the influence of plasma reactor structure and catalysts on CO_2 conversion and CH_3OH selectivity for plasma catalytic CO_2 hydrogenation [125], and a schematic diagram of the experimental setup and images of the H_2/CO_2 discharge are shown in Figure 22. They investigated three kinds of reactors, i.e., a cylindrical reactor (aluminum foil sheet as ground electrode), a double dielectric barrier discharge reactor (water as ground electrode), and a single dielectric barrier discharge reactor (water as a ground electrode). The single DBD reactor equipped with a special water-electrode showed the optimal reaction performance (21.2% CO_2 conversion and 53.7% CH_3OH selectivity). In addition, they tested the catalytic performance of Pt/γ-Al_2O_3 catalysts and Cu/γ-Al_2O_3 catalysts in the optimized reactor for direct conversion of CO_2 to CH_3OH. As shown in Figure 23, both Pt/γ-Al_2O_3 catalysts and Cu/γ-Al_2O_3 catalysts improved not only the CO_2 conversion, but also the CH_3OH selectivity, and Cu/γ-Al_2O_3 catalysts showed a better catalytic performance (21.2% CO_2 conversion and 53.7% methanol selectivity). That is, a strong synergistic effect between the plasma and Cu/γ-Al_2O_3 catalysts promoted the hydrogenation of CO_2 to methanol, although the reaction temperature in the optimized reactor remained near room temperature.

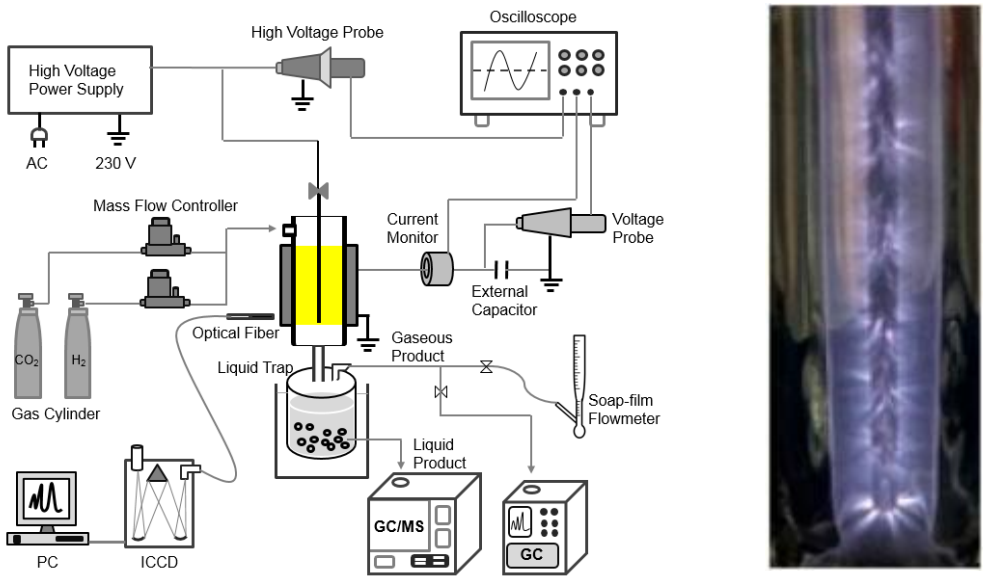

(**a**) (**b**)

Figure 22. (**a**) Schematic diagram of the experimental setup of a DBD plasma catalytic reactor. (**b**) Images of H_2/CO_2 discharge generated in DBD reactor without catalyst, reprinted with permission from [125]. Copyright American Chemical Society, 2017.

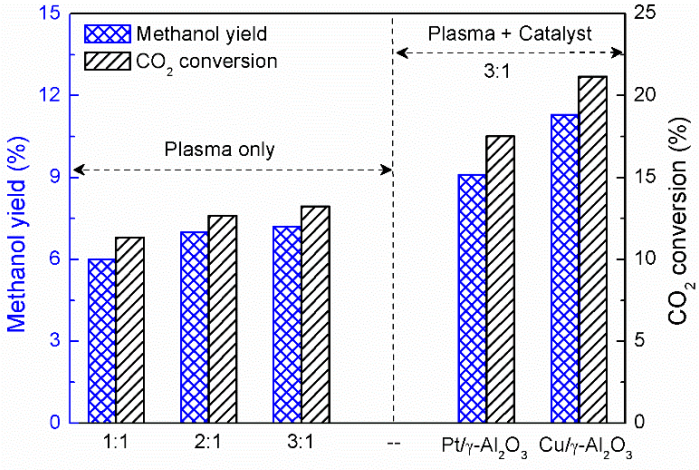

Figure 23. Effect of H_2/CO_2 molar ratio and catalysts on the reaction performance of the plasma hydrogenation process, reprinted with permission from [125]. Copyright American Chemical Society, 2017.

It is obvious that the combination of the plasma and catalysts can enhance the catalytic reaction at room temperature and atmospheric pressure. The maximum methanol selectivity of 53.7% was achieved with a CO_2 conversion of 21.2% via the plasma-catalysis process (see Figure 23). All the above studies show a strong synergistic effect between plasma and catalysts.

Using one-dimensional fluid modeling [126], De Bie et al. proposed a chemical reaction network in the plasma (i.e., without catalysts) for conversion of CO_2 to value-added chemicals, i.e., CO, CH_4, CH_2O, CH_3OH, and hydrocarbons. The simulation results indicated the dominant reaction pathways for the conversion of CO_2 and H_2, as illustrated in Scheme 5. According to the model, the combination between H atoms and CHO radicals is the most important reaction to form CO, while this reaction is counterbalanced by the reorganization of H with CO into CHO radicals. Therefore, the most effective net CO formation reaction is dissociation of CO_2 influenced by electrons. The production of CH_4 was generally driven by two reactions, i.e., three-body recombination reaction between CH_3 and H radicals, and charge transfer reaction between CH_5^+ and H_2O. However, the latter reaction is partly balanced by the loss of CH_4, resulting from a charge transfer reaction with H_3^+. The production of CH_2O is closely related to the initial CO_2 fraction in the gas mixture. At a low initial fraction of CO_2, the reaction between CO_2 and CH_2 radicals seem to be the most important channel for the formation of CH_2O, while at higher initial CO_2 fractions, CH_2O is also produced out of two CHO radicals to some extent. In addition, as predicted by the model, the most important channel for the formation of CH_3OH is the three-body reaction between CH_3 and OH radicals, while the three-body reaction between CH_2OH and H radicals is also an effective production channel for CH_3OH. Furthermore, they also found that a higher density of CH_3 and CH_2 radicals would be essential to tune the distribution of end products. Therefore, it can be predicted that the degree of hydrogenation in the reaction has a significant influence for the targeted products.

Figure 24 summarizes the selectivity of CO, CH_4, or CH_3OH, as a function of the CO_2 conversion, obtained from the recent reports discussed above. Several main trends are clear. Firstly, the main products are CO and CH_4 for direct hydrogenation of CO_2 in plasma catalysis, while the selectivity of CH_3OH is relatively low. Moreover, it is obvious that researchers have paid more attention to the reduction of CO_2 to CO and CH_4 up to now. However, the production of other hydrocarbons, such as olefins and gasoline hydrocarbons, would also be a promising direction, to achieve the maximum utilization of CO_2 by plasma catalysis. Therefore, some insights from heterogeneous catalysis, especially the combination of metal catalysts, metal oxide catalysts, and zeolite catalysts could be helpful to develop a methodology for plasma catalytic hydrogenation of CO_2. On the other hand, there is no guarantee that good catalysts in thermal processes would also perform well in plasma

catalysis, because of the clearly different operating conditions (e.g., lower temperature, abundance of reactive species, excited species, charges, and electric field present in plasma).

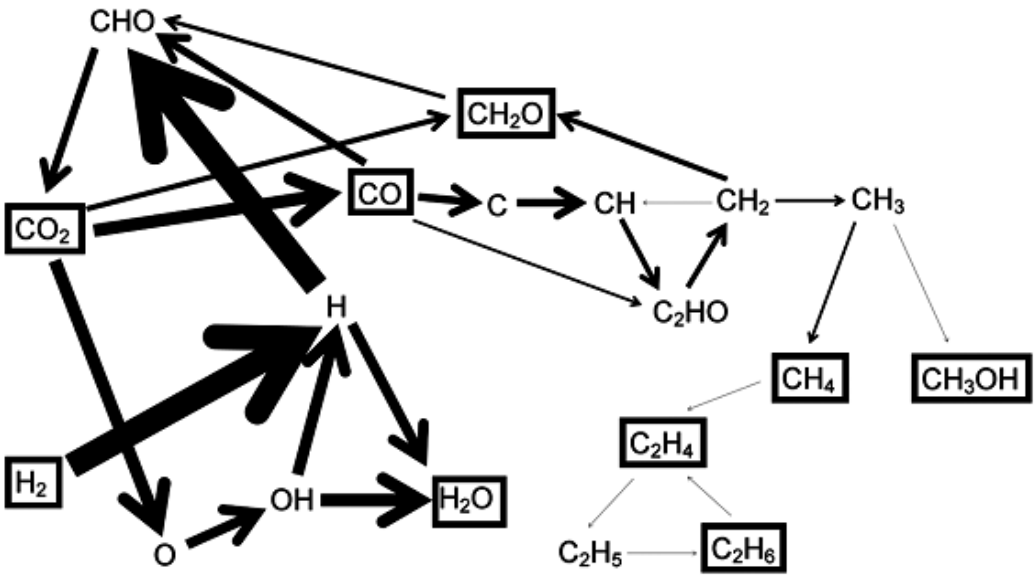

Scheme 5. Dominant reaction pathways for the plasma-based conversion (without catalysts) of CO_2 and H_2 into various products, in a 50/50 CO_2/H_2 gas mixture. The thickness of the arrow lines is proportional to the rates of the net reactions. The stable molecules are indicated with black rectangles, reprinted with permission from [126]. Copyright American Chemical Society, 2016.

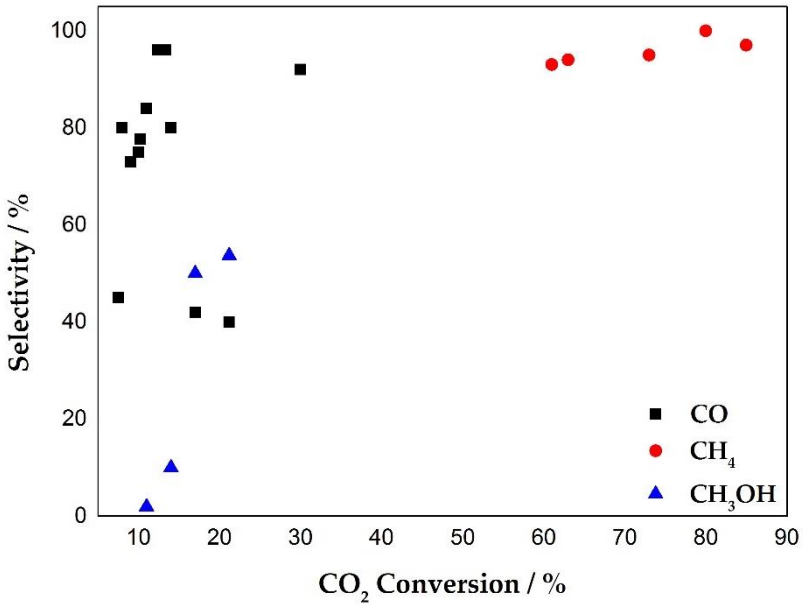

Figure 24. Overview of selectivity into CO, CH_4, and CH_3OH, as a function of CO_2 conversion, based on all reports available in literature about plasma catalysis (all in DBD reactors). The references where these data are adopted from are discussed in the text.

Up to now, in view of the complexity of this interdisciplinary field, the development of plasma catalysis still needs major research efforts. On one hand, plasma catalysis has potential for industrial application, because it drives the CO_2 conversion reaction at ambient temperature and atmospheric pressure, breaking thermodynamic equilibrium to make full use of feedstock. On the other hand,

the excessive energy consumption—caused by high input power and heat loss—is an important disadvantage, but it can be mitigated with the further development of renewable energy (i.e., wind, solar, and tidal energy). Additionally, to improve the reaction activity for CO_2 conversion, it is crucial to explore the reaction mechanisms by in situ characterization and computer modeling, to improve the synergistic effect between plasma and catalysts. Finally, we need to search for suitable catalytic materials to strength the reaction performance and decrease the production costs.

4. Outlook and Conclusions

Currently, fuels and base chemicals are nearly all produced from non-renewable fossil energy (oil, natural gas, and coal), and CO_2 is generally the end product (e.g., upon burning fossil fuels) or a waste product in chemical industry. This indicates that we should use CO_2 as the main carbon source when fossil energy would get depleted in the future. Thus, in the long term, hydrogenation of CO_2 (as well as CO_2 conversion with other H-sources) into value-added chemicals and fuels is very significant, since it can close the carbon cycle, as shown in Figure 25. However, some crucial issues should be addressed in advance for application of CO_2 hydrogenation in industry.

Figure 25. CO_2 conversion into fuels, which release CO_2 again upon burning, aiming a closed carbon cycle.

From a relatively economical point of view, the direct hydrogenation of CO_2 is not yet a viable approach. On one hand, CO_2 of a certain purity generally depends on the development of capture and separation techniques. On the other hand, compared with the price of the feedstock (H_2, 10,000 \$/ton), the price of the main products (i.e., liquefied natural gas, 770 \$/ton, and CH_3OH, 340 \$/ton) obtained by CO_2 hydrogenation is too low to make this an economically viable process. However, once the production of H_2 can be realized with fully-fledged solar power technology, the production cost for CO_2 hydrogenation will be greatly reduced. Meanwhile, the CO_2 conversion driven by solar energy (artificial photosynthesis) is also a promising routing.

Technologically, the direct hydrogenation of CO_2 to CO is an endothermic reaction ($\Delta H = 41.2$ kJ mol^{-1}), and a higher reaction temperature is beneficial for the production of CO according to Le Chatelier's principle. Based on the available experimental results (Table 1), the CO selectivity can reach nearly 100% under conditions of 873 K and 1 MPa. On the other hand, the production of other products (i.e., CH_4, CH_3OH, DME, and light olefins) from CO_2 is exothermic, and in theory a low temperature favors the equilibrium conversion. However, the inert CO_2 molecule generally needs relatively high reaction temperature to be activated. The competition between these two factors makes the reaction performance not very satisfactory. Up to now, from the perspective of technology

readiness level, methanol synthesis is a far more advanced production process, with a high selectivity up to 80–90% with Cu-based catalyst (Table 3). However, there are some limitations in heterogeneous catalysis for direct hydrogenation of CO_2, such as catalyst sintering at high temperature, the influence of water produced in the reaction process and low CO_2 conversion caused by thermo-dynamical restriction in terms of the formation of CH_3OH and hydrocarbons. Hence, we should explore novel catalytic materials and reactors to break the thermodynamic equilibrium, as well as design bi-functional and/or multi-functional catalysts (metal, metal oxides, and zeolites) to couple the chemical reactions (RWGS, methanation, methanol synthesis, and/or MTO).

Plasma catalysis, a new field of catalysis, has attracted sufficient attention in recent years, due to its simple operating conditions (ambient temperature and atmospheric pressure) and unique advantages in activating inert molecules. However, the energy efficiency is still too high for commercial exploitation. On the other hand, renewable energy (e.g., wind, solar, and tidal energy) will further develop in the near future, and it will be a perfect match with plasma catalysis (because plasma is generated by electricity and can simply be switched on/off—allowing storage of fluctuating energy), hence making the problem of limited energy efficiency less dramatic. Nevertheless, significant efforts must be devoted to elucidate the reaction mechanisms in plasma catalysis, to improve not only the energy efficiency, but certainly also the selectivity towards value-added products. Indeed, plasma catalysis is complicated from chemistry and physics point of view, but the potential of plasma technology for industrial applications deserves major research efforts. A combination of computer simulations with experiments will be needed for an in-depth understanding of the reaction mechanisms, responsible for the synergy between plasma and catalysts. Although the development process in plasma catalysis may be slow due to its complex character, it would bring great benefits to human society, once it is developed mature enough, and once appropriate catalysts for plasma catalysis can be designed. Therefore, future research should definitely emphasize on a better understanding and rational screening of highly active catalysts.

Compared with the numerous studies on CO_2 hydrogenation by heterogeneous catalysis, much more research should be carried out in the field of plasma catalysis, to improve the CO_2 conversion and target products selectivity (and even to exploit new products, such as olefins, gasoline hydrocarbons, and aromatics), since the results achieved by plasma catalysis (Figure 24) are far from those of heterogeneous catalysis (Figure 18). To achieve this goal, the advantage of plasma should be exploited in full, and at the same time, insights from heterogeneous catalysis (e.g., catalyst combination, reaction combination, active sites design, etc.) can help to further improve the potential of this promising field of catalysis.

Author Contributions: Conceptualization: M.L., Y.Y., L.W. and A.B.; Validation: M.L., Y.Y., L.W., H.G. and A.B.; Formal analysis: M.L., Y.Y., L.W., H.G. and A.B.; Resources: Y.Y. and A.B.; Data curation: Y.Y., L.W. and A.B.; Writing—original draft preparation: M.L. and Y.Y.; Writing—review and editing: Y.Y. and A.B.; Supervision: Y.Y., L.W. and A.B.; Funding acquisition: Y.Y. and A.B.

Funding: This research was funded by the Fundamental Research Funds for the Central Universities of China (DUT18JC42), the National Natural Science Foundation of China (21503032), PetroChina Innovation Foundation (2018D-5007-0501), and the TOP research project of the Research Fund of the University of Antwerp (32249).

Conflicts of Interest: The authors declare no conflict of interest.

References

1. Ingwersen, W.W.; Garmestani, A.S.; Gonzalez, M.A.; Templeton, J.J. A systems perspective on responses to climate change. *Clean Technol. Environ. Policy* **2014**, *16*, 719–730. [CrossRef]
2. Wang, W.; Wang, S.; Ma, X.; Cong, J. Recent advances in catalytic hydrogenation of carbon dioxide. *Chem. Soc. Rev.* **2011**, *40*, 3703–3727. [CrossRef] [PubMed]
3. Irish, J.L.; Sleath, A.; Cialone, M.A.; Knutson, T.R.; Jensen, R.E. Simulations of Hurricane Katrina (2005) under sea level and climate conditions for 1900. *Clim. Chang.* **2014**, *122*, 635–649. [CrossRef]

4. Sanz-perez, E.S.; Murdock, C.R.; Didas, S.A.; Jones, C.W. Direct Capture of CO_2 from Ambient Air. *Chem. Rev.* **2016**, *116*, 11840–11876. [CrossRef] [PubMed]
5. Boot-Handford, M.E.; Abanades, J.C.; Anthony, E.J.; Blunt, M.J.; Brandani, S.; Dowell, N.M. Carbon capture and storage update. *Energy Environ. Sci.* **2014**, *7*, 130–189. [CrossRef]
6. Bui, M.; Adjiman, C.S.; Bardow, A.; Anthony, E.J.; Boston, A.; Brown, S.; Fennell, P.S.; Fuss, S. Carbon capture and storage (CCS): The way forward. *Energy Environ. Sci.* **2018**, *11*, 1062–1176. [CrossRef]
7. Bobicki, E.R.; Liu, Q.; Xu, Z.; Zeng, H. Carbon capture and storage using alkaline industrial wastes. *Prog. Energy Combust. Sci.* **2012**, *38*, 302–320. [CrossRef]
8. Rahman, F.A.; Aziz, M.M.A.; Saidur, R.; Wan, W.A.; Hainin, M.R.; Putrajava, R.; Hassan, N.A. Pollution to solution: Capture and sequestration of carbon dioxide (CO_2) and its utilization as a renewable energy source for a sustainable future. *Renew. Sustain. Energy Rev.* **2017**, *71*, 112–126. [CrossRef]
9. Darabi, A.; Jessop, P.G.; Cunningham, M.F. CO_2-responsive polymeric materials: Synthesis, self-assembly, and functional applications. *Chem. Soc. Rev.* **2016**, *45*, 4391–4436. [CrossRef]
10. Dincer, I.; Acar, C. Review and evaluation of hydrogen production methods for better sustainability. *Int. J. Hydrogen Energy* **2015**, *40*, 11094–11111. [CrossRef]
11. Centi, G.; Quadrelli, E.A.; Perathoner, S. Catalysis for CO_2 conversion: A key technology for rapid introduction of renewable energy in the value chain of chemical industries. *Energy Environ. Sci.* **2013**, *6*, 1711–1731. [CrossRef]
12. Álvarez, A.; Bansode, A.; Urakawa, A.; Bavykina, A.V.; Wezendonk, T.A.; Makkee, M.; Gascon, J.; Kapteijn, F. Challenges in the Greener Production of Formates/Formic Acid, Methanol, and DME by Heterogeneously Catalyzed CO_2 Hydrogenation Processes. *Chem. Rev.* **2017**, *117*, 9804–9838. [CrossRef]
13. Snoeckx, R.; Bogaerts, A. Plasma technology—A novel solution for CO_2 conversion? *Chem. Soc. Rev.* **2017**, *46*, 5805–5863. [CrossRef]
14. Dalle, K.E.; Warnan, J.; Leung, J.J.; Reuillard, B.; Karmel, I.S.; Reisner, E. Electro- and Solar-Driven Fuel Synthesis with First Row Transition Metal Complexes. *Chem. Rev.* **2018**. [CrossRef]
15. Li, X.; Yu, J.G.; Jaroniec, M.; Chen, X.B. Cocatalysts for Selective Photoreduction of CO_2 into Solar Fuels. *Chem. Rev.* **2018**. [CrossRef]
16. Mota, F.M.; Kim, D.H. From CO_2 methanation to ambitious long-chain hydrocarbons: Alternative fuels paving the path to sustainability. *Chem. Soc. Rev.* **2019**, *48*, 205–259. [CrossRef]
17. Jadhav, S.G.; Vaidya, P.D.; Bhanage, B.M.; Joshi, J.B. Catalytic carbon dioxide hydrogenation to methanol: A review of recent studies. *Chem. Eng. Res. Des.* **2014**, *92*, 2557–2567. [CrossRef]
18. Porosoff, M.D.; Yan, B.; Chen, J.G. Catalytic reduction of CO_2 by H_2 for synthesis of CO, methanol and hydrocarbons: Challenges and opportunities. *Energy Environ. Sci.* **2016**, *9*, 62–73. [CrossRef]
19. Bando, K.K.; Soga, K.; Kunimori, K.; Ichikuni, N.; Okabe, K.; Kusama, H.; Sayama, K.; Arakawea, H. CO_2 hydrogenation activity and surface structure of zeolite-supported Rh catalysts. *Appl. Catal. A* **1998**, *173*, 47–60. [CrossRef]
20. Porosoff, M.D.; Yang, X.; Boscoboinik, J.A.; Chen, J.G. Molybdenum Carbide as Alternative Catalysts to Precious Metals for Highly Selective Reduction of CO_2 to CO. *Angew. Chem. Int. Ed.* **2014**, *53*, 6705–6709. [CrossRef]
21. Kattel, S.; Yan, B.; Chen, J.G.; Liu, P. CO_2 hydrogenation on Pt, Pt/SiO_2 and Pt/TiO_2: Importance of synergy between Pt and oxide support. *J. Catal.* **2016**, *343*, 115–126. [CrossRef]
22. Yan, Y.; Wang, Q.; Jiang, C.; Yao, Y.; Lu, D.; Zheng, J.; Dai, Y.; Wang, H.; Yang, Y. Ru/Al_2O_3 catalyzed CO_2 hydrogenation: Oxygen-exchange on metal-support interfaces. *J. Catal.* **2018**, *367*, 194–205. [CrossRef]
23. Yan, B.; Wu, Q.; Cen, J.; Timoshenko, J.; Frenkel, A.I.; Su, D.; Chen, X.; Parise, J.B.; Stach, E.; Orlov, A.; et al. Highly active subnanometer Rh clusters derived from Rh-doped $SrTiO_3$ for CO_2 reduction. *Appl. Catal. B* **2018**, *237*, 1003–1011. [CrossRef]
24. Dai, B.; Cao, S.; Xie, H.; Zhou, G.; Chen, S. Reduction of CO_2 to CO via reverse water-gas shift reaction over CeO_2 catalyst. *Korean J. Chem. Eng.* **2018**, *35*, 421–427. [CrossRef]
25. Alayoglu, S.; Beaumont, S.K.; Zheng, F.; Pushkarev, V.V.; Zheng, H.; Iablokov, V.; Liu, Z.; Guo, J.; Kruse, N.; Somorjai, G.A. CO_2 Hydrogenation Studies on Co and CoPt Bimetallic Nanoparticles Under Reaction Conditions Using TEM, XPS and NEXAFS. *Top. Catal.* **2011**, *54*, 778–785. [CrossRef]
26. Kharaji, A.G.; Shariati, A.; Takassi, M.A. A Novel γ-Alumina Supported Fe-Mo Bimetallic Catalyst for Reverse Water Gas Shift Reaction. *Chin. J. Chem. Eng.* **2013**, *21*, 1007–1014. [CrossRef]

27. Kharaji, A.G.; Shariati, A.; Ostadi, M. Development of Ni–Mo/Al_2O_3 Catalyst for Reverse Water Gas Shift (RWGS) Reaction. *J. Nanosci. Nanotechnol.* **2014**, *14*, 6841–6847. [CrossRef]
28. Zhao, B.; Yan, B.; Jiang, Z.; Yao, S.; Liu, Z.; Wu, Q.; Ran, R.; Senanayake, S.D.; Weng, D.; Chen, J.G. High selectivity of CO_2 hydrogenation to CO by controlling the valence state of nickel using perovskite. *Chem. Commun.* **2018**, *54*, 7354–7357. [CrossRef]
29. Quindimil, A.; De-La-Torre, U.; Pereda-Ayo, B.; González-Marcos, J.A.; González-Velasco, J.R. Ni catalysts with La as promoter supported over Y- and BETA-zeolites for CO_2 methanation. *Appl. Catal. B* **2018**, *238*, 393–403. [CrossRef]
30. Zhou, G.; Wu, T.; Xie, H.; Zheng, X. Effects of structure on the carbon dioxide methanation performance of Co-based catalysts. *Int. J. Hydrogen Energy* **2013**, *38*, 10012–10018. [CrossRef]
31. Lin, Q.; Liu, X.Y.; Jiang, Y.; Wang, Y.; Huang, Y.; Zhang, T. Crystal phase effects on the structure and performance of ruthenium nanoparticles for CO_2 hydrogenation. *Catal. Sci. Technol.* **2014**, *4*, 2058–2063. [CrossRef]
32. Yuan, H.; Zhu, X.; Han, J.; Wang, H.; Ge, Q. Rhenium-promoted selective CO_2 methanation on Ni-based catalyst. *J. CO_2 Util.* **2018**, *26*, 8–18. [CrossRef]
33. Li, M.; Amari, H.; van Veen, A.C. Metal-oxide interaction enhanced CO_2 activation in methanation over ceria supported nickel nanocrystallites. *Appl. Catal. B* **2018**, *239*, 27–35. [CrossRef]
34. Zhan, Y.; Wang, Y.; Gu, D.; Chen, C.; Jiang, L.; Takehira, K. Ni/Al_2O_3-ZrO_2 catalyst for CO_2 methanation: The role of γ-(Al, Zr)$_2O_3$ formation. *Appl. Surf. Sci.* **2018**, *459*, 74–79. [CrossRef]
35. Ma, H.; Ma, K.; Ji, J.; Tang, S.; Liu, C.; Jiang, W.; Yue, H.; Liang, B. Graphene intercalated Ni-SiO_2/GO-Ni-foam catalyst with enhanced reactivity and heat-transfer for CO_2 methanation. *Chem. Eng. Sci.* **2019**, *194*, 10–21. [CrossRef]
36. Romero-Sáez, M.; Dongil, A.B.; Benito, N.; Espinoza-González, R.; Escalona, N.; Gracia, F. CO_2 methanation over nickel-ZrO_2 catalyst supported on carbon nanotubes: A comparison between two impregnation strategies. *Appl. Catal. B* **2018**, *237*, 817–825. [CrossRef]
37. Bacariza, M.C.; Graça, I.; Lopes, J.M.; Henriques, C. Ni-Ce/Zeolites for CO_2 Hydrogenation to CH_4: Effect of the Metal Incorporation Order. *ChemCatChem* **2018**, *10*, 2773–2781. [CrossRef]
38. Liu, H.; Xu, S.; Zhou, G.; Huang, G.; Huang, S.; Xiong, K. CO_2 hydrogenation to methane over Co/KIT-6 catalyst: Effect of reduction temperature. *Chem. Eng. J.* **2018**, *351*, 65–73. [CrossRef]
39. Zhou, G.; Liu, H.; Xing, Y.; Xu, S.; Xie, H.; Xiong, K. CO_2 hydrogenation to methane over mesoporous Co/SiO_2 catalysts: Effect of structure. *J. CO_2 Util.* **2018**, *26*, 221–229. [CrossRef]
40. Gnanakumar, E.S.; Chandran, N.; Kozhevnikov, I.V.; Grau-Atienza, A.; Ramos Fernández, E.V.; Sepulveda-Escribano, A.; Shiju, N.R. Highly efficient nickel-niobia composite catalysts for hydrogenation of CO_2 to methane. *Chem. Eng. Sci.* **2019**, *194*, 2–9. [CrossRef]
41. Olah, G.A.; Goeppert, A.; Surya Prakash, G.K. Beyond oil and gas: The methanol Economy. *Angew. Chem. Int. Ed.* **2005**, *44*, 2636–2639. [CrossRef]
42. Li, W.; Lu, P.; Xu, D.; Tao, K. CO_2 hydrogenation to methanol over Cu/ZnO catalysts synthesized via a facile solid-phase grinding process using oxalic acid. *Korean J. Chem. Eng.* **2018**, *35*, 110–117. [CrossRef]
43. Cao, F.H.; Liu, D.H.; Hou, Q.S.; Fang, D.Y. Thermodynamic Analysis of CO_2 Direct Hydrogenation Reactions. *J. Nat. Gas Chem.* **2001**, *10*, 24–33.
44. Deng, K.; Hu, B.; Lu, Q.; Hong, X. Cu/g-C_3N_4 modified ZnO/Al_2O_3 catalyst: Methanol yield improvement of CO_2 hydrogenation. *Catal. Commun.* **2017**, *100*, 81–84. [CrossRef]
45. Witoon, T.; Numpilai, T.; Phongamwong, T.; Donphai, W.; Boonyuen, C.; Warakulwit, C.; Chareonpanich, M.; Limtrakul, J. Enhanced activity, selectivity and stability of a CuO-ZnO-ZrO_2 catalyst by adding graphene oxide for CO_2 hydrogenation to methanol. *Chem. Eng. J.* **2018**, *334*, 1781–1791. [CrossRef]
46. Wang, G.; Mao, D.; Guo, X.; Yu, J. Enhanced performance of the CuO-ZnO-ZrO_2 catalyst for CO_2 hydrogenation to methanol by WO_3 modification. *Appl. Surf. Sci.* **2018**, *456*, 403–409. [CrossRef]
47. Ye, J.; Liu, C.; Mei, D.; Ge, Q. Active Oxygen Vacancy Site for Methanol Synthesis from CO_2 Hydrogenation on In_2O_3(110): A DFT Study. *ACS Catal.* **2013**, *3*, 1296–1306. [CrossRef]
48. Sun, K.; Fan, Z.; Ye, J.; Yan, J.; Ge, Q.; Li, Y.; He, W.; Yang, W.; Liu, C. Hydrogenation of CO_2 to methanol over In_2O_3 catalyst. *J. CO_2 Util.* **2015**, *12*, 1–6. [CrossRef]

49. Martin, O.; Martin, A.J.; Mondelli, C.; Mitchell, S.; Segawa, T.F.; Hauert, R.; Drouilly, C.; Curulla-Ferre, D.; Perez-Ramirez, J. Indium Oxide as a Superior Catalyst for Methanol Synthesis by CO_2 Hydrogenation. *Angew. Chem. Int. Ed.* **2016**, *55*, 6261–6265. [CrossRef]
50. Wang, J.; Li, G.; Li, Z.; Tang, C.; Feng, Z.; An, H.; Liu, H.; Liu, T.; Li, C. A highly selective and stable ZnO-ZrO_2 solid solution catalyst for CO_2 hydrogenation to methanol. *Sci. Adv.* **2017**, *3*, e1701290. [CrossRef]
51. Jiang, X.; Jiao, Y.; Moran, C.; Nie, X.; Gong, Y.; Guo, X.; Walton, K.S.; Song, C. CO_2 hydrogenation to methanol on Pd-Cu bimetallic catalysts with lower metal loadings. *Catal. Commun.* **2019**, *118*, 10–14. [CrossRef]
52. Jiang, X.; Wang, X.; Nie, X.; Koizumi, N.; Guo, X.; Song, C. CO_2 hydrogenation to methanol on Pd-Cu bimetallic catalysts: H_2/CO_2 ratio dependence and surface species. *Catal. Today* **2018**, *316*, 62–70. [CrossRef]
53. Bahruji, H.; Esquius, J.R.; Bowker, M.; Hutchings, G.; Armstrong, R.D.; Jones, W. Solvent Free Synthesis of PdZn/TiO_2 Catalysts for the Hydrogenation of CO_2 to Methanol. *Top. Catal.* **2018**, *61*, 144–153. [CrossRef]
54. Yin, Y.; Hu, B.; Li, X.; Zhou, X.; Hong, X.; Liu, G. Pd@zeolitic imidazolate framework-8 derived PdZn alloy catalysts for efficient hydrogenation of CO_2 to methanol. *Appl. Catal. B* **2018**, *234*, 143–152. [CrossRef]
55. Hu, B.; Yin, Y.; Liu, G.; Chen, S.; Hong, X.; Tsang, S.C.E. Hydrogen spillover enabled active Cu sites for methanol synthesis from CO_2 hydrogenation over Pd doped CuZn catalysts. *J. Catal.* **2018**, *359*, 17–26. [CrossRef]
56. Studt, F.; Sharafutdinov, I.; Abild-Pedersen, F.; Elkjær, C.F.; Hummelshøj, J.S.; Dahl, S.; Chorkendorff, I.; Nørskov, J.K. Discovery of a Ni-Ga catalyst for carbon dioxide reduction to methanol. *Nat. Chem.* **2014**, *6*, 320–324. [CrossRef]
57. Marcos, F.C.F.; Assaf, J.M.; Assaf, E.M. CuFe and CuCo supported on pillared clay as catalysts for CO_2 hydrogenation into value-added products in one-step. *Mol. Catal.* **2018**, *458*, 297–306. [CrossRef]
58. Joseph, A.S.; Can, A.; Julia, S.; Wang, T.; Jens, K.N.; Frank, A.P.; Stacey, F.B. Theoretical and Experimental Studies of CoGa Catalysts for the Hydrogenation of CO_2 to Methanol. *Catal. Lett.* **2018**, *148*, 3583–3591.
59. Tan, Q.; Shi, Z.; Wu, D. CO_2 Hydrogenation to Methanol over a Highly Active Cu–Ni/CeO_2–Nanotube Catalyst. *Ind. Eng. Chem. Res.* **2018**, *57*, 10148–10158. [CrossRef]
60. Jiang, Y.; Yang, H.; Gao, P.; Li, X.; Zhang, J.; Liu, H.; Wang, H.; Wei, W.; Sun, Y. Slurry methanol synthesis from CO_2 hydrogenation over micro-spherical SiO_2 support Cu/ZnO catalysts. *J. CO_2 Util.* **2018**, *26*, 642–651. [CrossRef]
61. Chen, P.; Zhao, G.; Liu, Y.; Lu, Y. Monolithic $Ni_5Ga_3/SiO_2/Al_2O_3$/Al-fiber catalyst for CO_2 hydrogenation to methanol at ambient pressure. *Appl. Catal. A* **2018**, *562*, 234–240. [CrossRef]
62. Lam, E.; Larmier, K.; Wolf, P.; Tada, S.; Safonova, O.V.; Copéret, C. Isolated Zr Surface Sites on Silica Promote Hydrogenation of CO_2 to CH_3OH in Supported Cu Catalysts. *J. Am. Chem. Soc.* **2018**, *140*, 10530–10535. [CrossRef]
63. Dasireddy, V.D.B.C.; Stefancic, N.S.; Likozar, B. Correlation between synthesis pH, structure and $Cu/MgO/Al_2O_3$ heterogeneous catalyst activity and selectivity in CO_2 hydrogenation to methanol. *J. CO_2 Util.* **2018**, *28*, 189–199. [CrossRef]
64. Shi, Z.; Tan, Q.; Wu, D. Ternary copper-cerium-zirconium mixed metal oxide catalyst for direct CO_2 hydrogenation to methanol. *Mater. Chem. Phys.* **2018**, *219*, 263–272. [CrossRef]
65. Bao, Y.; Huang, C.; Chen, L.; Zhang, Y.D.; Liang, L.; Wen, J.; Fu, M.; Wu, J.; Ye, D. Highly efficient Cu/anatase TiO_2 {001}-nanosheets catalysts for methanol synthesis from CO_2. *J. Energy Chem.* **2018**, *27*, 381–388. [CrossRef]
66. Koh, M.K.; Khavarian, M.; Chai, S.P.; Mohamed, A.R. The morphological impact of siliceous porous carriers on copper-catalysts for selective direct CO_2 hydrogenation to methanol. *Int. J. Hydrogen Energy* **2018**, *43*, 9334–9342. [CrossRef]
67. Tasfy, S.; Zabidi, N.A.M.; Shaharum, M.S.; Subbarao, D. Methanol production via CO_2 hydrogenation reaction: Effect of catalyst support. *Int. J. Nanotechnol.* **2017**, *14*, 410–421. [CrossRef]
68. Li, Y.; Na, W.; Wang, H.; Gao, W. Hydrogenation of CO_2 to methanol over Au–CuO/SBA-15 catalysts. *J. Porous Mater.* **2017**, *24*, 591–599. [CrossRef]
69. Atakan, A.; Mäkie, P.; Söderlind, F.; Keraudy, J.; Björk, E.M.; Odén, M. Synthesis of a Cu-infiltrated Zr-doped SBA-15 catalyst for CO_2 hydrogenation into methanol and dimethyl ether. *Phys. Chem. Chem. Phys.* **2017**, *19*, 19139–19149. [CrossRef]
70. Rui, N.; Wang, Z.; Sun, K.; Ye, J.; Ge, Q.; Liu, C. CO_2 hydrogenation to methanol over Pd/In_2O_3: Effects of Pd and oxygen vacancy. *Appl. Catal. B* **2017**, *218*, 488–497. [CrossRef]

71. Zhang, J.; Lu, S.; Su, X.; Fan, S.; Ma, Q.; Zhao, T. Selective formation of light olefins from CO_2 hydrogenation over Fe–Zn–K catalysts. *J. CO_2 Util.* **2015**, *12*, 95–100. [CrossRef]
72. You, Z.; Deng, W.; Zhang, Q.; Wang, Y. Hydrogenation of carbon dioxide to light olefins over non-supported iron catalyst. *Chin. J. Catal.* **2013**, *34*, 956–963. [CrossRef]
73. Gao, P.; Li, S.; Bu, X.; Dang, S.; Liu, Z.; Wang, H.; Zhong, L.; Qiu, M.; Yang, C.; Cai, J.; et al. Direct conversion of CO_2 into liquid fuels with high selectivity over a bifunctional catalyst. *Nat. Chem.* **2017**, *9*, 1019–1024. [CrossRef] [PubMed]
74. Xie, C.; Chen, C.; Yu, Y.; Su, J.; Li, Y.; Somorjai, G.A.; Yang, P. Tandem Catalysis for CO_2 Hydrogenation to C_2–C_4 Hydrocarbons. *Nano Lett.* **2017**, *17*, 3798–3802. [CrossRef]
75. Li, S.; Guo, H.; Luo, C.; Zhang, H.; Xiong, L.; Chen, X.; Ma, L. Effect of Iron Promoter on Structure and Performance of K/Cu–Zn Catalyst for Higher Alcohols Synthesis from CO_2 Hydrogenation. *Catal. Lett.* **2013**, *143*, 345–355. [CrossRef]
76. Wei, J.; Yao, R.; Ge, Q.; Wen, Z.; Ji, X.; Fang, C.; Zhang, J.; Xu, H.; Sun, J. Catalytic Hydrogenation of CO_2 to Isoparaffins over Fe-Based Multifunctional Catalysts. *ACS Catal.* **2018**, *8*, 9958–9967. [CrossRef]
77. Li, Z.; Qu, Y.; Wang, J.; Liu, H.; Li, M.; Miao, S.; Li, C. Highly Selective Conversion of Carbon Dioxide to Aromatics over Tandem Catalysts. *Joule* **2019**, *3*, 1–14. [CrossRef]
78. Ni, Y.; Chen, Z.; Fu, Y.; Liu, Y.; Zhu, W.; Liu, Z. Selective conversion of CO_2 and H_2 into aromatics. *Nat. Commun.* **2018**, *9*, 3457. [CrossRef] [PubMed]
79. Zhang, M.H.; Liu, Z.M.; Lin, G.D.; Zhang, H.B. Pd/CNT-promoted $CuZrO_2$/HZSM-5 hybrid catalysts for direct synthesis of DME from CO_2/H_2. *Appl. Catal. A* **2013**, *451*, 28–35. [CrossRef]
80. Wu, T.; Lin, J.; Cheng, Y.; Tian, J.; Wang, S.; Xie, S.; Pei, Y.; Yan, S.; Qiao, M.; Xu, H.; et al. Porous Graphene-Confined Fe–K as Highly Efficient Catalyst for CO_2 Direct Hydrogenation to Light Olefins. *ACS Appl. Mater. Interfaces* **2018**, *10*, 23439–23443. [CrossRef]
81. Zhang, Y.; Li, D.; Zhang, Y.; Cao, Y.; Zhang, S.; Wang, K.; Ding, F.; Wu, J. V-modified CuO–ZnO–ZrO_2/HZSM-5 catalyst for efficient direct synthesis of DME from CO_2 hydrogenation. *Catal. Commun.* **2014**, *55*, 49–52. [CrossRef]
82. Gao, W.; Wang, H.; Wang, Y.; Guo, W.; Jia, M. Dimethyl ether synthesis from CO_2 hydrogenation on La-modified CuO-ZnO-Al_2O_3/HZSM-5 bifunctional catalysts. *J. Rare Earths* **2013**, *31*, 470–476. [CrossRef]
83. Suwannapichat, Y.; Numpilai, T.; Chanlek, N.; Faungnawakij, K.; Chareonpanich, M.; Limtrakul, J.; Witoon, T. Direct synthesis of dimethyl ether from CO_2 hydrogenation over novel hybrid catalysts containing a Cu-ZnO-ZrO_2 catalyst admixed with WO_x/Al_2O_3 catalysts: Effects of pore size of Al_2O_3 support and W loading content. *Energy Convers. Manag.* **2018**, *159*, 20–29. [CrossRef]
84. Michailos, S.; McCord, S.; Sick, V.; Stokes, G.; Styring, P. Dimethyl ether synthesis via captured CO_2 hydrogenation within the power to liquids concept: A techno-economic assessment. *Energy Convers. Manag.* **2019**, *184*, 262–276. [CrossRef]
85. Quadrelli, E.A.; Centi, G.; Duplan, J.L.; Perathoner, S. Carbon Dioxide Recycling: Emerging Large-Scale Technologies with Industrial Potential. *ChemSusChem* **2011**, *4*, 1194–1215. [CrossRef] [PubMed]
86. Cho, W.; Song, T.; Mitsos, A.; McKinnon, J.T.; Ko, G.H.; Tolsma, J.E.; Denholm, D.; Park, T. Optimal design and operation of a natural gas tri-reforming reactor for DME synthesis. *Catal. Today* **2009**, *139*, 261–267. [CrossRef]
87. Hirano, M.; Tatsumi, M.; Yasutake, T.; Kuroda, K. Dimethyl ether synthesis via reforming of steam/carbon dioxide and methane. *J. Jpn. Pet. Inst.* **2005**, *48*, 197–203. [CrossRef]
88. Hirano, M.; Yasutake, T.; Kuroda, K. Dimethyl ether synthesis from carbon dioxide by catalytic hydrogenation (Part 3) direct synthesis using hybrid by recycling process. *J. Jpn. Pet. Inst.* **2007**, *50*, 34–43. [CrossRef]
89. Bonura, G.; Migliori, M.; Frusteri, L.; Cannilla, C.; Catizzone, E.; Giordano, G.; Frusteri, F. Acidity control of zeolite functionality on activity and stability of hybrid catalysts during DME production via CO_2 hydrogenation. *J. CO_2 Util.* **2018**, *24*, 398–406. [CrossRef]
90. Catizzone, E.; Migliori, M.; Purita, A.; Giordano, G. Ferrierite vs. γ-Al_2O_3: The superiority of zeolites in terms of water-resistance in vapour-phase dehydration of methanol to dimethyl ether. *J. Energy Chem.* **2019**, *30*, 162–169. [CrossRef]
91. Catizzone, E.; Bonura, G.; Migliori, M.; Frusteri, F.; Giordano, G. CO_2 Recycling to Dimethyl Ether: State-of-the-Art and Perspectives. *Molecules* **2018**, *23*, 31. [CrossRef] [PubMed]

92. De Falco, M.; Capocelli, M.; Centi, G. Dimethyl ether production from CO_2 rich feedstocks in a one-step process: Thermodynamic evaluation and reactor simulation. *Chem. Eng. J.* **2016**, *294*, 400–409. [CrossRef]
93. Fang, J.; Jin, X.F.; Huang, K. Life cycle analysis of a combined CO_2 capture and conversion membrane reactor. *J. Membr. Sci.* **2018**, *549*, 142–150. [CrossRef]
94. Sofia, D.; Giuliano, A.; Poletto, M.; Barletta, D. Techno-economic analysis of power and hydrogen co-production by an IGCC plant with CO_2 capture based on membrane technology. *Comput. Aided Process Eng.* **2015**, *37*, 1373–1378.
95. Li, Z.; Wang, J.; Qu, Y.; Liu, H.; Tang, C.; Miao, S.; Feng, Z.; An, H.; Li, C. Highly Selective Conversion of Carbon Dioxide to Lower Olefins. *ACS Catal.* **2017**, *7*, 8544–8548. [CrossRef]
96. Da Silva, R.J.; Pimentel, A.F.; Monteiro, R.S.; Mota, C.J.A. Synthesis of methanol and dimethyl ether from the CO_2 hydrogenation over Cu·ZnO supported on Al_2O_3 and Nb_2O_5. *J. CO_2 Util.* **2016**, *15*, 83–88. [CrossRef]
97. Dang, S.; Gao, P.; Liu, Z.; Chen, X.; Yang, C.; Wang, H.; Zhong, L.; Li, S.; Sun, Y. Role of zirconium in direct CO_2 hydrogenation to lower olefins on oxide/zeolite bifunctional catalysts. *J. Catal.* **2018**, *364*, 382–393. [CrossRef]
98. Wang, P.; Zha, F.; Yao, L.; Chang, Y. Synthesis of light olefins from CO_2 hydrogenation over (CuO-ZnO)-kaolin/SAPO-34 molecular sieves. *Appl. Clay Sci.* **2018**, *163*, 249–256. [CrossRef]
99. Guo, L.; Sun, J.; Ji, X.; Wei, J.; Wen, Z.; Yao, R.; Xu, H.; Ge, Q. Directly converting carbon dioxide to linear α-olefins on bio-promoted catalysts. *Commun. Chem.* **2018**, *1*, 11. [CrossRef]
100. Bonura, G.; Cordaro, M.; Spadaro, L.; Cannilla, C.; Arena, F.; Frusteri, F. Hybrid Cu–ZnO–ZrO_2/H-ZSM5 system for the direct synthesis of DME by CO_2 hydrogenation. *Appl. Catal. B* **2013**, *140–141*, 16–24. [CrossRef]
101. Bonura, G.; Cordaro, M.; Cannilla, C.; Mezzapica, A.; Spadaro, L.; Arena, F.; Frusteri, F. Catalytic behaviour of a bifunctional system for the one step synthesis of DME by CO_2 hydrogenation. *Catal. Today* **2014**, *228*, 51–57. [CrossRef]
102. Zhang, Y.; Li, D.; Zhang, S.; Wang, K.; Wu, J. CO_2 hydrogenation to dimethyl ether over CuO–ZnO–Al_2O_3/HZSM-5 prepared by combustion route. *RSC Adv.* **2014**, *4*, 16391–16396. [CrossRef]
103. Zha, F.; Tian, H.; Yan, J.; Chang, Y. Multi-walled carbon nanotubes as catalyst promoter for dimethyl ether synthesis from CO_2 hydrogenation. *Appl. Surf. Sci.* **2013**, *285*, 945–951. [CrossRef]
104. Frusteri, F.; Bonura, G.; Cannilla, C.; Drago Ferrante, G.; Aloise, A.; Catizzone, E.; Migliori, M.; Giordano, G. Stepwise tuning of metal-oxide and acid sites of CuZnZr-MFI hybrid catalysts for the direct DME synthesis by CO_2 hydrogenation. *Appl. Catal. B* **2015**, *176–177*, 522–531. [CrossRef]
105. Liu, R.; Tian, H.; Yang, A.; Zha, F.; Ding, J.; Chang, Y. Preparation of HZSM-5 membrane packed CuO–ZnO–Al_2O_3 nanoparticles for catalysing carbon dioxide hydrogenation to dimethyl ether. *Appl. Surf. Sci.* **2015**, *345*, 1–9. [CrossRef]
106. Dai, C.; Zhang, A.; Liu, M.; Li, J.; Song, F.; Song, C.; Guo, X. Facile one-step synthesis of hierarchical porous carbon monoliths as superior supports of Fe-based catalysts for CO_2 hydrogenation. *RSC Adv.* **2016**, *6*, 10831–10836. [CrossRef]
107. Wei, J.; Ge, Q.; Yao, R.; Wen, Z.; Fang, C.; Guo, L.; Xu, H.; Sun, J. Directly converting CO_2 into a gasoline fuel. *Nat. Commun.* **2017**, *8*, 16170. [CrossRef]
108. Liu, J.; Zhang, A.; Jiang, X.; Liu, M.; Zhu, J.; Song, C.; Guo, X. Direct Transformation of Carbon Dioxide to Value-Added Hydrocarbons by Physical Mixtures of Fe_5C_2 and K-Modified Al_2O_3. *Ind. Eng. Chem. Res.* **2018**, *57*, 9120–9126. [CrossRef]
109. Zhang, J.; Su, X.; Wang, X.; Ma, Q.; Fan, S.; Zhao, T.S. Promotion effects of Ce added Fe–Zr–K on CO_2 hydrogenation to light olefins. *React. Kinet. Mech. Catal.* **2018**, *124*, 575–585. [CrossRef]
110. Ramirez, A.; Gevers, L.; Bavykina, A.; Ould-Chikh, S.; Gascon, J. Metal Organic Framework-Derived Iron Catalysts for the Direct Hydrogenation of CO_2 to Short Chain Olefins. *ACS Catal.* **2018**, *8*, 9174–9182. [CrossRef]
111. Shi, Z.; Yang, H.; Gao, P.; Chen, X.; Liu, H.; Zhong, L.; Wang, H.; Wei, W.; Sun, Y. Effect of alkali metals on the performance of CoCu/TiO_2 catalysts for CO_2 hydrogenation to long-chain hydrocarbons. *Chin. J. Catal.* **2018**, *39*, 1294–1302. [CrossRef]
112. Bogaerts, A.; Neyts, E.; Gijbels, R.; van der Mullen, J. Gas discharge plasmas and their applications. *Spectrochim. Acta Part B* **2002**, *57*, 609–658. [CrossRef]
113. Bogaerts, A.; Neyts, E.C. Plasma Technology: An Emerging Technology for Energy Storage. *ACS Energy Lett.* **2018**, *3*, 1013–1027. [CrossRef]

114. Paulussen, S.; Verheyde, B.; Tu, X.; De Bie, C.; Martens, T.; Petrovic, D.; Bogaerts, A.; Sels, B. Conversion of carbon dioxide to value-added chemicals in atmospheric pressure dielectric barrier discharges. *Plasma Sources Sci. Technol.* **2010**, *19*, 034015. [CrossRef]
115. Silva, T.; Britun, N.; Godfroid, T.; Snyders, R. Optical characterization of a microwave pulsed discharge used for dissociation of CO_2. *Plasma Sources Sci. Technol.* **2014**, *23*, 25009. [CrossRef]
116. Ozkan, A.; Dufour, T.; Silva, T.; Britun, N.; Snyders, R.; Reniers, F.; Bogaerts, A. DBD in burst mode: Solution for more efficient CO_2 conversion? *Plasma Sources Sci. Technol.* **2016**, *25*, 055005. [CrossRef]
117. Wang, W.; Berthelot, A.; Kolev, S.; Tu, X.; Bogaerts, A. CO_2 conversion in a gliding arc plasma: 1D cylindrical discharge model. *Plasma Sources Sci. Technol.* **2016**, *25*, 065012. [CrossRef]
118. Li, D.; Li, X.; Bai, M.; Tao, X.; Shang, S.; Dai, X.; Yin, Y. CO_2 reforming of CH_4 by atmospheric pressure glow discharge plasma: A high conversion ability. *Int. J. Hydrogen Energy* **2009**, *34*, 308–313. [CrossRef]
119. Liu, J.L.; Park, H.W.; Chung, W.J.; Park, D.W. High-Efficient Conversion of CO_2 in AC-Pulsed Tornado Gliding Arc Plasma. *Plasma Chem. Plasma Process.* **2016**, *36*, 437–449. [CrossRef]
120. Kolb, T.; Voigt, J.H.; Gericke, K.H. Conversion of Methane and Carbon Dioxide in a DBD Reactor: Influence of Oxygen. *Plasma Chem. Plasma Process.* **2013**, *33*, 631–646. [CrossRef]
121. Wang, L.; Yi, Y.; Wu, C.; Guo, H.; Tu, X. One-Step Reforming of CO_2 and CH_4 into High-Value Liquid Chemicals and Fuels at Room Temperature by Plasma-Driven Catalysis. *Angew. Chem. Int. Ed.* **2017**, *56*, 13679–13683. [CrossRef]
122. Zhang, K.; Eliasson, B.; Kogelschatz, U. Direct Conversion of Greenhouse Gases to Synthesis Gas and C_4 Hydrocarbons over Zeolite HY Promoted by a Dielectric-Barrier Discharge. *Ind. Eng. Chem. Res.* **2002**, *41*, 1462–1468. [CrossRef]
123. Eliasson, B.; Kogelschatz, U.; Xue, B.; Zhou, L.M. Hydrogenation of Carbon Dioxide to Methanol with a Discharge-Activated Catalyst. *Ind. Eng. Chem. Res.* **1998**, *37*, 3350–3357. [CrossRef]
124. Zeng, Y.; Tu, X. Plasma-Catalytic CO_2 Hydrogenation at Low Temperatures. *IEEE Trans. Plasma Sci.* **2016**, *44*, 405–411. [CrossRef]
125. Wang, L.; Yi, Y.; Guo, H.; Tu, X. Atmospheric Pressure and Room Temperature Synthesis of Methanol through Plasma-Catalytic Hydrogenation of CO_2. *ACS Catal.* **2018**, *8*, 90–100. [CrossRef]
126. De Bie, C.; van Dijk, J.; Bogaerts, A. CO_2 Hydrogenation in a Dielectric Barrier Discharge Plasma Revealed. *J. Phys. Chem. C* **2016**, *120*, 25210–25224. [CrossRef]